H19 contributes to aerobic glycolysis, proliferation and immune escape of gastric cancer cells via the miR-519d-3p/LDHA axis

Linqing Sun
The First Affiliated Hospital of Soochow University
Juntao Li
The First Affiliated Hospital of Soochow University
Wenying Yan
Soochow University
Zhendong Yao
The First Affiliated Hospital of Soochow University
Ruoqin Wang
The First Affiliated Hospital of Soochow University
Xiaojun Zhou
The First Affiliated Hospital of Soochow University
Hongya Wu
The First Affiliated Hospital of Soochow University
Guangbo Zhang
The First Affiliated Hospital of Soochow University
Tongguo Shi (shitg@suda.edu.cn)
First Affiliated Hospital of Soochow University
Weichang Chen
The First Affiliated Hospital of Soochow University

Research

Keywords: Gastric cancer, H19, aerobic glycolysis, miR-519d-3p/LDHA axis, immune escape

Posted Date: October 29th, 2020

DOI: https://doi.org/10.21203/rs.3.rs-97859/v1

Abstract

Background Long non-coding RNAs (lncRNAs) have been investigated in multiple human cancers including gastric cancer (GC). Our research aims to explore the role of H19 in aerobic glycolysis, proliferation, and immune escape of GC cells.

Methods The expression of H19 in GC samples were analyzed using Gene Expression Profiling Interactive Analysis (GEPIA), Gene Expression Omnibus (GEO) data, and real-time quantitative polymerase chain reaction (RT-qPCR) analysis. Glucose consumption and lactate production were applied to assess the aerobic glycolysis of GC cells. Subcellular fractionation, luciferase reporter, and western blot assays certified the binding between genes. CCK-8 and colony formation assays were used to determine GC cell proliferation. Flow cytometry, ELISA, and RT-qPCR assays were applied to analyze the immunosuppressive effect of H19.

Results H19 was highly expressed in samples of patients with GC, and associated with tumor growth in vivo. H19 knockdown suppressed glucose consumption, lactate production, proliferation of GC cells by regulating miR-519d-3p/LDHA axis. Both miR-519d-3p depletion and LDHA overexpression could reverse the H19 knockdown-induced decrease in aerobic glycolysis and proliferation. Moreover, conditioned medium (CM) from stable knockdown H19 GC cells modulated the activity of immune cells including γδT cells, Jurkat cells, and tumor-associated macrophages (TAMs) in a lactate dependent manner.

Conclusions The H19/miR-519d-3p/LDHA axis mainly contributed to aerobic glycolysis, proliferation, and immune escape of GC cells.

Background

Gastric cancer (GC) ranked the fifth in prevalence and the third in mortality around the world according to the 2018 Global Cancer Statistics analysis [1]. Although the endoscopy, surgery and standard chemotherapy improved the 5-year survival rate of GC patients, the patients with advanced stages and metastasis had the unfavorable prognosis [2]. Consequently, it is worth seeking out new therapeutic targets and clarifying the pathogenesis of GC.

Long non-coding RNA (lncRNA) is a type of longer than 200 nucleotides RNA without protein-coding function [3]. As shown in recent studies, lncRNAs were implicated in multiple human cancers and involved in diverse biological processes of cancers, such as growth, metastasis, drug resistance, metabolism, and immune escape [4–7]. Among the lncRNAs associated with tumor progression, H19 is one of the most well-characterized lncRNAs. A large and growing body of literature has shown that H19 was overexpressed and served as an oncogene in diverse tumors, including breast cancer, colorectal cancer, pancreatic cancer, and GC [8–12]. Zhang, E et al. noted that H19 was overexpressed in GC tissues compared with adjacent normal tissues, and positively correlated with poor overall survival time [13]. Furthermore, studies have revealed that H19 exerted crucial roles in the regulation of GC cell proliferation,

migration, and invasion [14, 15]. However, many undefined molecular mechanisms by which H19 contributes to the progression of GC need to be thoroughly investigated.

As a distinctive hallmark of cancer, the Warburg effect or aerobic glycolysis confers on cancer cells a growth advantage by providing energy and biosynthesis building blocks even in the presence of abundant oxygen [16]. Aerobic glycolysis is now widely accepted and served as anti-tumor therapeutic target [17], but the molecular mechanisms controlling aerobic glycolysis have not been elucidated. Accumulated evidence has indicated that lncRNAs could regulate glucose metabolism in cancer cells by directly regulating the glycolytic enzymes and glucose transporters, or indirectly modulating the signaling pathways [18]. For instance, lncRNA AGPG enhanced glycolysis activity and cell proliferation in esophageal squamous cell carcinoma by stabilizing PFKFB3 [19]. Zhao and his coworkers noted that lncRNA MACC1-AS1 promoted GC cell metabolic plasticity via AMPK/Lin28 mediated mRNA stability of MACC1 [20]. Although increased H19 got involved in glycolysis and stemness maintenance in breast cancer stem cells via the let-7/HIF-1α/PDK1 pathway signaling cascade [21], the effect of H19 on aerobic glycolysis in GC remains largely unknown.

Mounting evidence suggested that aerobic glycolysis in cancer cells has the ability to regulate the immune response in the tumor microenvironment [22, 23]. Lactate, a kind of glycolytic metabolites, has been identified as a crucial component that contributes to the immunosuppressive tumor microenvironment [24]. Brand et al. showed that tumor-secreted lactate could dampen interferon-γ (IFN-γ) production by CD8 + T and NK cells and inhibiting their cytolytic activity [25]. Nonetheless, the link connecting H19, aerobic glycolysis, and immune escape in GC cells remains not fully characterized.

In this study, we investigated whether and how H19 modulated aerobic glycolysis, cell proliferation and immune evasion. Our results showed that the levels of H19 were increased significantly in GC tissue specimens and associated with poor prognosis. We further demonstrated that H19 knockdown suppressed aerobic glycolysis and cell proliferation through the miR-519d-3p/LDHA axis in GC cells. Moreover, H19 knockdown modified the activity of γδ T cells, T cells and tumor-associated macrophages (TAMs), which participate in tumor immune response, in a lactate dependent manner.

Methods

Clinical tissue specimens

Twelve paired fresh GC tissue specimens and adjacent normal tissue specimens from patients were obtained from the First Affiliated Hospital of Soochow University (Suzhou, China) between May 2017 and August 2018. All tissue specimens were snap-frozen in liquid nitrogen. This study was approved by the Institutional Review Board of the First Affiliated Hospital of Soochow University. Written informed consent was obtained from each patient. Basic information of clinical tissue specimens are provided in Supplementary Table 1.

Cell culture

Human GC lines AGS, SGC-7901, and MKN-45, normal gastric mucosa cell GES-1, Jurkat, and THP-1 cells were purchased from the Chinese Academy of Science Cell Bank (Shanghai, China). All cells were cultured in RPMI-1640 (Biological Industries, BeitHaemek, Israel) supplemented with 10% fetal bovine serum (FBS, Biological Industries) and 1% Penicillin -streptomycin (Beyotime, Shanghai, China, #C0222) in a humidified incubator with 5% CO_2 at 37°C.

Cell transfection

Two small interfering RNAs (siRNA) targeting human H19 (siRNA-1, and siRNA-2), were obtained from RiboBio Life Science Co., Ltd. (Guangzhou, China). Negative control (NC), miR-519d-3p mimic and miR-519d-3p inhibitor were purchased from Genepharma Co., Ltd. (Shanghai, China). pReceiver-Lv105-LDHA (LDHA) plasmid and pReceiver-Lv105-negative control plasmid were purchased from Gene Copoeia (Guangzhou, China). SGC-7901 and MKN-45 cells were transfected with siRNA reagents or plasmids using Lipofectamine 2000 (Invitrogen, Carlsbad, CA, USA) according to the manufacturer's instructions.

Lentiviral infection

Lentivirus vectors carrying human H19 shRNA and negative control lentivirus vectors were manufactured by Genepharma Co., Ltd. (Shanghai, China). For lentivirus infection, SGC-7901 and MKN-45 cells were infected with lentiviral particles at a multiplicity of infection (MOI) of 25. The efficiency of infection was confirmed by counting GFP-expressing cells under a fluorescence microscope.

RNA isolation and real-time quantitative polymerase chain reaction (RT-qPCR)

Total RNA from tissue samples or cells was extracted using TRIzol reagent (TaKaRa, Shiga, Japan) according to the manufacturer's instructions. For gene expression analysis, a total of 1 μg RNA was reverse-transcribed into cDNA using PrimeScript RT Master Mix (Takara, Shiga, Japan, #RR036A). RT-qPCR reactions were performed on a CFX96 Touch^{TM} real-time PCR system (Bio-Rad, CA, USA) using AceQ universal SYBR qPCR Master Mix (Vazyme, Nanjing, China, #Q511) according to the manufacturer's instructions. For miRNA expression analysis, 1 μg of total RNA was used for first-strand DNA synthesis using a miRNA 1st Strand cDNA Synthesis Kit (Vazyme, #MR101-02) and RT-qPCR was conducted using a miRNA universal SYBR qPCR Master Mix kit (Vazyme, #MQ101-02). Sample and reference genes were analyzed in triplicates. Individual gene expression was normalized to β-actin, while miRNA expression was normalized to small nuclear RNA U6. The primer sequences for RT-qPCR are provided in Supplementary Table 2.

Western Blot analysis

Cells were lysed with RIPA buffer (Beyotime, #P0013D) supplemented with protease inhibitors and phosphatase inhibitors (Beyotime, #P1045). Protein concentrations were examined with an Enhanced BCA Protein Assay Kit (Beyotime, #P0010). Total protein (30 μg) was separated by sodium dodecylsulfate-polyacrylamide gel electrophoresis (SDS-PAGE, Beyotime, #P0012AC) and transferred

onto polyvinylidene fluoride (PVDF) membranes (GE Healthcare Life science, Germany). The membranes were blocked with 5% BSA (Fcmacs, Nanjing, China, #FMS-WB021) for 1.5 h and then incubated with the rabbit anti-human/rabbit LDHA (Beyotime, AF1660), mouse anti-human/mouse β-actin (CST, #3700) at 4 °C overnight. On the following day, the membranes were incubated with the corresponding HRP-conjugated goat anti-rabbit or anti-mouse secondary antibodies (Beyotime) for 1 h at room temperature. The protein bands were visualized with ECL reagents (NCM Biotech, Suzhou, China, #10100) in a Chemi Doc^{TM} MP Imaging System (Bio-Rad). The band density was analyzed using ImageJ software.

Glucose consumption and lactate production assay

The glucose and lactate levels were measured using a glucose assay kit (robio, Shanghai, China, #361510) and a lactate assay kit (Jiancheng, Nanjing, China, #A019-2-1) following the manufacturer's protocols.

CCK-8 assay

The cell proliferation was assessed at 0, 24, 48 and 72 hours using Cell Counting Kit-8 (CCK-8) assay (Dojindo, Kumamoto, Japan, #CK04). Briefly, Cells were plated into 96-well plates at a density of $3´10^3$ cells per well. Then, 10ul CCK8 solution was added to each well and cells were incubated for another 2 h at 37°C. The optical density (OD) at 450nm was measured. Each group contained 5 replicates and all experiments were performed in triplicate.

Colony formation assay

Cells were seeded into 6-well plates at $1´10^3$ cells per well and cultured in a humidified incubator with 5% CO_2 at 37°C for 10-14 days. The cell colonies were fixed in methanol for 30 min and then stained with 1% crystal violet (Sigma) for 30 min. Then, the colonies were imaged and counted.

Cytoplasm and nuclear localization

Cytoplasm and nuclear were separated from the cells using Minute^{TM} Cytoplasmic and Nuclear Extraction Kit (inventbiotech, USA, #SC-003) according to the manufacturer's instructions.

Luciferase reporter assay

PmirGLO vectors containing the wild type (WT) or mutant (MUT) H19 or LDHA 3'UTR were obtained from Realgene Biotech (Nanjing, China). Luciferase reporter assay was performed following the previous protocols [26]. Briefly, MKN-45 cells were cultured in a 12-well plate and co-transfected with WT or MUT luciferase plasmids and miR-519d-3p mimic or control miRNA using Lipofectamine 2000. 24h after transfection, the cells were lysed with Passive Lysis Buffer (Promega, Madison, USA, #E1910), and the luciferase activity was measured with a Dual Luciferase Reporter Assay System (Promega, #E1910) according to the manufacturer's instructions.

Flow cytometry assay

For intracellular staining of IFN-γ, γδT cells were treated with CM or CM+lactate (Sanjia, Suzhou, China, #SL017769) for 24h, and stimulated with Cell Activation Cocktail with Brefeldin A (Biolegend, USA, #423304) for 10h. The cells were stained with PC7-conjugated antibody against CD3 (Biolegend) and FITC-conjugated antibody against γδT (Biolegend) at 4°C for 20 minutes. Then the cells were fixed and permeabilized with a Fixation/Permeabilization Solution Kit (BD Biosciences, #554714) according to the manufacturer's instructions, and stained with PE-conjugated antibody against IFN-γ (Biolegend) allowing analysis by a flow cytometry analyzer (Beckman Coulter).

Enzyme-linked immunosorbent assay (ELISA)

The concentrations of human IL-2 in the supernatants of Jurkat cells were examined with ELISA Kit (NeoBioscience, Shenzhen, China, #EHC003.96) according to the manufacturer's instructions.

Tumor-associated macrophages (TAMs) induction

THP-1 cells (1.5×10^5 cells/ml) were treated with 200 ng/ml phorbol myristate acetate (PMA, Solarbio Science & Technology Co., Ltd, Beijing, China.) for 24 h and polarized into macrophages [27]. To induce TAMs, THP-1 macrophages were cultured with CM of GC cells for a further 24h prior to harvesting.

Xenograft tumor

Six-eight-weeks-old female BALB/c athymic nude mice were purchased from the Shanghai Laboratory Animal Center. All animal experiments were approved by the Institutional Animal Care and Use Committee of Soochow University (Suzhou, China). All the mice were randomly divided into two groups (n=4 each group). $5´10^6$ MKN-45 cells with or without H19 knockdown were subcutaneously injected into the layer of the right flank of the mice. Tumor volume (mm^3) was calculated according to the following equation: V (mm^3) = $S^2(mm^2)$ × L(mm)/2, where S and L are the smallest and the largest perpendicular tumor diameters, respectively [28]. After 21 days, mice were sacrificed and the xenograft tumor tissues were removed, photographed and weighted.

Conditioned medium

Cells (3×10^5) were seeded in 6-well plates and cultured overnight. The culture medium was changed to fresh medium in each well. After 24 h, the conditioned medium (CM) was collected.

γδT cell separation and culture

γδT cells were isolated from human peripheral blood mononuclear cells (PBMCs) and cultured as our previously described [29].

Statistical analysis

All data were presented as mean ± SD. Student's *t*-test was used for comparisons between two groups. For survival curves, Kaplan-Meier method with log-rank or Gehan-Breslow-Wilcoxon test was used. Significant differences were displayed as follows: *p<0.05, **p<0.01, ***p<0.001 and ns. not significant.

Results

H19 was overexpression in GC tissue specimens and promoted tumor growth in nude mice.

Based on a new database visualization website of GEPIA with TCGA data (http://gepia.cancer-pku.cn/), the expression of H19 was significantly increased in GC tissue samples compared to normal samples (Fig. 1a). GSE2685 and GSE13861 microarray data from Gene Expression Omnibus (GEO) databases (http://www.ncbi.nlm.nih.gov/gds/) also showed that the H19 level was up-regulated in GC tissue samples (Fig. 1b). To corroborate the above results, we investigated the H19 expression level in 12 pairs of fresh GC tissues and corresponding normal adjacent tissues by RT-qPCR assay, and found that the relative expression of H19 was higher in tumor than that in normal tissues (Fig. 1c). We further evaluated the prognostic value of H19 in GC using GEPIA with TCGA data and GSE26253 microarray data. As shown in Fig. 1d, GC patients with high H19 expression had a shorter overall survival in TCGA data. Moreover, high expression of H19 predicted shorter recurrence-free survival in GSE26253 microarray data (Fig. 1e). Next, the expression of H19 in normal gastric mucosa cell GES-1 and three GC cell lines AGS, MKN-45, and SGC-7901 cells was examined. The RT-qPCR results noted that H19 was overexpression in GC cell lines (Fig. 1f).

We also established a nude-mouse xenograft tumor model using stable knockdown H19 MKN-45 cells to demonstrate the effect of H19 knockdown on tumor growth in vivo (**Fig. S1a-b and** Fig. 1g-i). The tumor sizes, images, and mass revealed that H19 knockdown significantly suppressed MKN-45 tumor growth (Fig. 1g-i). Collectively, these data demonstrated that H19 was highly expressed in a subset of patients with GC, and positively associated with tumor growth in vivo.

H19 knockdown inhibited glucose consumption and lactate production in gastric cancer cells.

Given that H19 could regulate aerobic glycolysis in breast cancer stem cells and ovarian cancer cells [21, 30], we hypothesized that H19 might be involved in the glycolysis process in gastric cancer cells. Hence, the H19 knockdown cell model was established by transfecting SGC-7901 and MKN-45 cells with two siRNAs (Fig. 2a). As shown in Fig. 2b, H19 depletion dramatically reduced the glucose consumption in SGC-7901 and MKN-45 cells. Moreover, we also analyzed the effect of H19 suppression on lactate production and found that the silencing of H19 significantly inhibited lactate production (Fig. 2c). Consistent with the above results, the glucose consumption and lactate production were also obviously decreased in stable knockdown H19 SGC-7901 or MKN-45 cells (Fig. 2d-e). These results indicated that H19 knockdown inhibited aerobic glycolysis in gastric cancer cells.

H19 regulated aerobic glycolysis through LDHA.

To elucidate the mechanisms that H19 knockdown suppressed aerobic glycolysis, a spectrum of key glycolysis-related genes were examined in H19 knockdown SGC-7901 and MKN-45 cells by RT-qPCR. The results showed that compared with GLUT1, LDHB, HK2, PKM2, and PDK1, the mRNA expression level of LDHA was positively correlated with the expression level of H19 in SGC-7901 and MKN-45 cells (Fig. 3a). Moreover, H19 knockdown reduced the protein expression of LDHA in SGC-7901 and MKN-45 cells (Fig. 3b **and Fig. S2a)**.

To explore whether LDHA contributed to H19-mediated glycolysis, we obtained a commercial LDHA overexpression plasmid (LDHA), which markedly up-regulated the LDHA protein level in SGC-7901 and MKN-45 cells (**Fig. S2b**). As shown in Fig. 3c, transfection with LDHA overexpression plasmid abolished the effect of H19 suppression on the protein expression of LDHA in SGC-7901 and MKN-45 cells (Fig. 3c, **Fig. S2c).** More importantly, LDHA overexpression reversed the H19 depletion-induced decrease in glucose consumption and lactate production (Fig. 3d-g**).**

H19 regulated LDHA expression and glycolysis in a miR-519d-3p dependent manner.

To explore how H19 regulated LDHA expression in gastric cancer cells, we performed cytoplasmic and nuclear separation experiments with RT-qPCR to determine the subcellular localization of H19 and LDHA. The results showed that H19 was distributed in both the nuclear and cytoplasm, while LDHA was predominantly localized in the cytoplasm (Fig. 4a). Moreover, the predicted results of lncATLAS (http://lncatlas.crg.eu/) also indicated that H19 was localized in both the nuclear and cytoplasm (**Fig. S3**). Therefore, we speculated that H19 may function as a competitive endogenous RNA (ceRNA) to regulate LDHA expression by sponging one or several specific miRNAs. Hence, we predicted the possible binding miRNAs of H19 and LDHA by using three publicly available prediction tools starbase3.0 (for H19), targetscan7.2 (for LDHA), and miRcode (for H19). As shown in Fig. 4b, three miRNAs (miR-519d-3p, miR-216b-5p and miR-17-5p) could bind to both H19 and LDHA. Subsequently, the levels of the three candidate miRNAs were detected by RT-qPCR, and the results revealed that miR-519d-3p expression was significantly increased in H19 knockdown SGC-7901 and MKN-45 cells (Fig. 4c). As shown in Fig. 4d, we showed the hybridization models between H19 and miR-519d-3p. Next, we performed luciferase reporter assays to determine whether miR-519d-3p could directly regulate H19. miR-519d-3p overexpression impaired the luciferase activity of the pmirGLO-H19-WT vector but failed to reduce that of the pmirGLO-H19-MUT vector (Fig. 4e). Moreover, the results of RT-qPCR in SGC-7901 and MKN-45 cells also indicated that the down-regulation of miR-519d-3p significantly increased the levels of H19, whereas miR-519d-3p overexpression reduced the levels of H19 (Fig. 4f**).**

The hybridization models between LDHA and miR-519d-3p were shown in Fig. 5a. Luciferase reporter assays confirmed the direct interaction between LDHA and miR-519d-3p. miR-519d-3p mimic reduced the luciferase activity of the pmirGLO-LDHA-WT vector but failed to decrease that of the pmirGLO-LDHA-MUT vector (Fig. 5b). miR-519d-3p knockdown elevated, whereas miR-519d-3p overexpression reduced, the mRNA and protein expression of LDHA in SGC-7901 and MKN-45 cells (Fig. 5c-d **and Fig. S4a**).

We further performed the rescue experiments. The results indicated that down-regulation of miR-519d-3p could counteract the increases in miR-519d-3p expression induced by H19 knockdown in SGC-7901 and MKN-45 cells (**Fig. S4b**). Additionally, miR-519d-3p inhibitor reversed the decreases in LDHA mRNA and protein expression in stable knockdown H19 SGC-7901 and MKN-45 cells (Fig. 5e-f, **Fig. S4c)**. Furthermore, miR-519d-3p knockdown abolished the effect of H19 suppression on glucose consumption and lactate production in SGC-7901 and MKN-45 cells (Fig. 5g-h**)**. These data suggested that H19 could modulate the LDHA expression and glycolysis by sponging miR-519d-3p.

H19 knockdown suppressed GC cell proliferation via the miR-519d-3p/LDHA axis.

Notably, H19 has been reported to promote cancer cell proliferation via multiple mechanisms [31–33]. Herein, we investigated the effect of H19 knockdown on GC cell proliferation and explored the underlying molecular mechanisms. CCK-8 assay indicated that H19 knockdown significantly decreased the proliferation rate of GC cells (Fig. 6a-b). These results were further confirmed by clonogenic assay (Fig. 6c-d). Given that H19 modulated glycolysis through regulating LDHA expression in a miR-519d-3p dependent manner, we thus next determined whether H19 was involved in GC cell growth via the miR-519d-3p/LDHA axis. Rescue experiments validated that the effect of H19 knockdown on GC cell proliferation rate and colony formation was reversed by miR-519d-3p depletion and LDHA overexpression (Fig. 6).

H19 signaling-mediated lactate production modulated immune escape.

Previous studies have shown that lactate, a major glycolytic metabolite, could modify tumor immune response [25, 34]. Also, our results indicated that H19 knockdown markedly decreased the accumulation of extracellular level of lactate (Fig. 2c and 2e). Therefore, we asked whether H19 was able to modulate tumor immune response in a lactate dependent manner. As shown in Fig. 7a, CM from stable knockdown H19 GC cells obviously elevated the population of IFN-γ-positive (IFN-γ+) γδT cells, an important anti-tumor immune cell [35]. Moreover, treatment with lactate counteracted the increases in the population of IFN-γ + γδT cells induced by conditioned medium from stable knockdown H19 GC cells (Fig. 7a**)**. Besides, the addition of lactate also reduced the IL-2 expression in PMA and Ionomycin-activated Jurkat cells, which was enhanced by CM from stable knockdown H19 GC cells (Fig. 7b).

We also investigated whether H19 signaling could modulate TAMs generation from human monocyte cell line THP-1. After treatment with PMA for 24 h, THP-1 cells were cultured with CM from stable knockdown H19 GC cells. The results of RT-qPCR showed that macrophages treated with CM from stable knockdown H19 GC cells exhibited higher levels of M1 marker NOS2, CXCL9, TNF-α and HLA-DR, while lower levels of M2 marker ARG1 and TGF-β (Fig. 7c). Treatment with lactate abolished the effect of conditioned medium from stable knockdown H19 GC cells on TAMs generation (Fig. 7c). The above results suggested that increased levels of extracellular lactate induced by H19 signaling modulated the activity of immune cells including γδT cells, Jurkat cells and TAMs, which might contribute to immune escape of GC cells.

Discussion

H19 has been identified to act as an important regulator in the tumorigenesis and progression of GC. For instance, up-regulated H19 was associated with lymph node metastasis and TNM stage of GC patients and promoted cell growth and metastasis via the miR-22-3p/Snail1 signaling pathway in GC [36]. H19-derived miR-675 was demonstrated to enhance the proliferation and invasion of GC cells via RUNX1 [37]. Herein, findings from our study were consistent with previous publications that H19 was highly expressed in GC tissues and associated with the poor prognosis of patients with GC. Using a nude-mouse xenograft tumor model, H19 knockdown was found to significantly suppress tumor growth in vivo. More importantly, we demonstrated that H19 modulated the aerobic glycolysis, proliferation, and immune escape of GC cells by sponging miR-519d-3p to induce the expression of LDHA (Fig. 8).

Previous studies noted that H19 participated in cancer cell aerobic glycolysis. The H19/let-7/HIF-1α signaling-mediated PDK1 could regulate glycolysis, and further contribute to breast cancer stem cell maintenance under hypoxic conditions [21]. In ovarian cancer, H19 overexpression increased glucose consumption, lactate production and PKM2 expression in SKOV3 and A2780 cells treated with ginsenoside 20(S)-Rg3 [30]. The above studies showed the important roles of H19 in the regulation of aerobic glycolysis in cancers, but the effect of H19 on aerobic glycolysis in GC remains largely unknown. In this study, we found that H19 knockdown decreased the glucose consumption and lactate production in SGC-7901 and MKN-45 cells. Aerobic glycolysis is driven by a spectrum of key glycolysis-related genes, including GLUT1, LDHB, LDHA, HK2, PKM2, and PDK1. Among these glycolysis-related genes, the mRNA and protein levels of LDHA were positively associated with H19 levels in both SGC-7901 and MKN-45 cells. Importantly, LDHA was highly expressed in GC samples [38, 39], and involved in glucose metabolism, proliferation, and migration of GC cells [40, 41]. Therefore, we inferred that H19 participated in GC aerobic glycolysis by regulating LDHA. The results of western blot indicated that LDHA overexpression abolished the effect of H19 suppression on the protein expression of LDHA in SGC-7901 and MKN-45 cells. More importantly, LDHA overexpression reversed the H19 depletion-induced decreases in glucose consumption and lactate production in SGC-7901 and MKN-45 cells. Our data suggested that the important effect of H19 on GC aerobic glycolysis is LDHA-dependent. Given that H19 was involved in regulating glycolysis in breast cancer stem cells under hypoxic conditions [21], we can not explain the roles of H19 in modulating aerobic glycolysis in GC cells under hypoxic conditions in the current study. Further investigations are required to answer this question.

It is well known that the lncRNAs' biological function is largely dependent on their subcellular localization [42]. Hence, to explore how H19 regulated LDHA expression in GC cells, we performed cytoplasmic and nuclear separation experiments with RT-qPCR analysis to determine the subcellular localization of H19 and LDHA. The results showed that H19 and LDHA were co-localized in the cytoplasm. Therefore, we speculated that H19 may function as a ceRNA to regulate LDHA expression by sponging one or several specific miRNAs. Subsequently, bioinformatics analysis indicated that miR-519d-3p, miR-216b-5p, and miR-17-5p could bind to both H19 and LDHA. Moreover, there was a negative correlation between miR-519d-3p and H19 or LDHA in GC cells. Importantly, miR-519d-3p functioned as a tumor suppressor in

multiple malignant tumors, such as colorectal cancer [43], breast cancer [44], pancreatic ductal adenocarcinoma [45], and GC [46]. Herein, in vitro luciferase assays indicated that both H19 and LDHA were direct targets of miR-519d-3p. Furthermore, we confirmed that miR-519d-3p overexpression decreased, while miR-519d-3p knockdown increased, the levels of H19 and LDHA in SGC-7901 and MKN-45 cells. Moreover, miR-519d-3p knockdown abolished the effect of H19 suppression on LDHA expression, glucose consumption, lactate production, and cell proliferation in GC cells. The above results revealed that H19 could regulate glycolysis and cell proliferation through the miR-519d-3p/LDHA axis.

As a major glycolytic metabolite, lactate functioned as a modulator of immune response and tumor progression [24, 25, 34]. LDHA-associated lactate accumulation blunted tumor surveillance by inhibiting the function and survival of T and NK cells [25]. Chen et al. indicated that lactate could activate macrophage G protein-coupled receptor 132 (Gpr132) to promote the alternatively activated macrophage (M2)-like phenotype [47]. Furthermore, lactate was markedly up-regulated in GC tumor-infiltrating T cells and associated with decreased T helper (Th)1 cell and cytotoxic T lymphocytes (CTLs) [48]. Based on our data that H19 affected the lactate accumulation, we concluded that H19 might modulate tumor immune response in a lactate dependent manner. Our and others' studies showed that γδT cells have important roles in tumor immunosurveillance against multiple malignancies such as colorectal cancer and leukemia [29, 49]. Importantly, tumor-infiltrating γδT cells were an independent prognostic factor in GC patients and could predict the survival benefit of adjuvant chemotherapy in patients with TNM II and III diseases [50]. Therefore, we explored the effect of CM from stable knockdown H19 GC cells on γδT cells. Our results indicated that CM from stable knockdown H19 GC cells elevated the population of IFN-γ + γδT cells, while lactate treatment counteracted this effect. In addition, we also asked whether CM from stable knockdown H19 GC cells could affect T cells and TAMs via lactate. The addition of lactate abolished the increase in IL-2 expression in PMA and Ionomycin-activated Jurkat cells induced by CM from stable knockdown H19 GC cells. Moreover, treatment with lactate reversed the effect of CM from stable knockdown H19 GC cells on TAMs generation. These data indicated that H19 signaling-mediated extracellular lactate accumulation could modulate the activity of immune cells including γδT cells, T cells, and TAMs, which might contribute to the immune escape of GC cells. Nevertheless, the effect of the H19/lactate axis on other immune cells, such as NK cells, myeloid-derived suppressor cells (MDSC), and Foxp3 regulatory T cells (Treg), are needed to investigate in our future study.

Conclusions

In summary, our results demonstrated the novel role of H19 in modulating aerobic glycolysis, proliferation, and immune escape of GC. Moreover, H19 mediated the effect on aerobic glycolysis, proliferation, and immune escape of GC cells via the miR-519d-3p/LDHA axis.

Abbreviations

LncRNA: Long noncoding RNA; GC: Gastric cancer; LDHA: Lactate dehydrogenase A; GEPIA: Gene Expression Profiling Interactive Analysis; TCGA: The Cancer Genome Atlas;

GEO: Gene Expression Omnibus; RT-qPCR: Real-time quantitative polymerase chain reaction; CCK-8: Cell Counting Kit-8; ELISA: Enzyme-linked immunosorbent assay; CM: Conditioned medium; TAMs: Tumor-associated macrophages; PVDF: Polyvinylidene fluoride; SD: Standard deviation

Declarations

Acknowledgements

Not applicable.

Authors' Contributions:

LQS, TGS and WCC designed the experiments; LQS performed most of the experiments; XJZ contributed to provide clinical samples; JTL, WYY, ZDY, RQW and HYW assisted with experiments and analysis of the data; WCC, GBZ provided administrative, technical, or material support. LQS and TGS wrote the manuscript. All authors read and approved the final manuscript.

Funding

This work was supported by The National Natural Science Foundation of China (81802843,82073156); Suzhou Science & Technology plan project (SYS2019035).

Availability of data and materials

The datasets used and analyzed during the current study are available from the corresponding author on reasonable request.

Ethics approval and consent to participate

With the informed consents signed by all patients, this study had received the approval of the Institutional Review Board of the First Affiliated Hospital of Soochow University.

Consent for publication

All authors reached an agreement to publish the study in this journal.

Competing interests

The authors declare that they have no competing interests.

References

1. Bray F, Ferlay J, Soerjomataram I, Siegel R, Torre L, and Jemal A. Global cancer statistics 2018: GLOBOCAN estimates of incidence and mortality worldwide for 36 cancers in 185 countries. CA: a cancer journal for clinicians, 2018; 68(6): 394-424.

2. Sexton R, Al Hallak M, Diab M, and Azmi A. Gastric cancer: a comprehensive review of current and future treatment strategies. Cancer metastasis reviews, 2020.
3. Begolli R, Sideris N, and Giakountis A. LncRNAs as Chromatin Regulators in Cancer: From Molecular Function to Clinical Potential. Cancers, 2019; 11(10).
4. Zhang H, Zhu C, He Z, Chen S, Li L, and Sun C. LncRNA PSMB8-AS1 contributes to pancreatic cancer progression via modulating miR-382-3p/STAT1/PD-L1 axis. Journal of experimental & clinical cancer research : CR, 2020; 39(1): 179.
5. Fang Z, Wang Y, Wang Z, Xu M, Ren S, Yang D, et al. ERINA is an estrogen-responsive lncRNA that drives breast cancer through the E2F1/RB1 pathway. Cancer research, 2020.
6. Gandhi M, Groß M, Holler J, Coggins S, Patil N, Leupold J, et al. The lncRNA lincNMR regulates nucleotide metabolism via a YBX1 - RRM2 axis in cancer. Nature communications, 2020; 11(1): 3214.
7. Zhang M, Wang N, Song P, Fu Y, Ren Y, Li Z, et al. LncRNA GATA3-AS1 facilitates tumour progression and immune escape in triple-negative breast cancer through destabilization of GATA3 but stabilization of PD-L1. Cell proliferation, 2020: e12855.
8. Wang J, Xie S, Yang J, Xiong H, Jia Y, Zhou Y, et al. The long noncoding RNA H19 promotes tamoxifen resistance in breast cancer via autophagy. Journal of hematology & oncology, 2019; 12(1): 81.
9. Zhang Y, Huang W, Yuan Y, Li J, Wu J, Yu J, et al. Long non-coding RNA H19 promotes colorectal cancer metastasis via binding to hnRNPA2B1. Journal of experimental & clinical cancer research : CR, 2020; 39(1): 141.
10. Yoshimura H, Matsuda Y, Yamamoto M, Michishita M, Takahashi K, Sasaki N, et al. Reduced expression of the H19 long non-coding RNA inhibits pancreatic cancer metastasis. Laboratory investigation; a journal of technical methods and pathology, 2018; 98(6): 814-824.
11. Yan J, Zhang Y, She Q, Li X, Peng L, Wang X, et al. Long Noncoding RNA H19/miR-675 Axis Promotes Gastric Cancer via FADD/Caspase 8/Caspase 3 Signaling Pathway. Cellular physiology and biochemistry : international journal of experimental cellular physiology, biochemistry, and pharmacology, 2017; 42(6): 2364-2376.
12. Lecerf C, Le Bourhis X, and Adriaenssens E. The long non-coding RNA H19: an active player with multiple facets to sustain the hallmarks of cancer. Cellular and molecular life sciences : CMLS, 2019; 76(23): 4673-4687.
13. Zhang E, Han L, Yin D, Kong R, De W, and Chen J. c-Myc-induced, long, noncoding H19 affects cell proliferation and predicts a poor prognosis in patients with gastric cancer. Medical oncology (Northwood, London, England), 2014; 31(5): 914.
14. Zhou X, Ye F, Yin C, Zhuang Y, Yue G, and Zhang G. The Interaction Between MiR-141 and lncRNA-H19 in Regulating Cell Proliferation and Migration in Gastric Cancer. Cellular physiology and biochemistry : international journal of experimental cellular physiology, biochemistry, and pharmacology, 2015; 36(4): 1440-52.

15. Li P, Tong L, Song Y, Sun J, Shi J, Wu Z, et al. Long noncoding RNA H19 participates in metformin-mediated inhibition of gastric cancer cell invasion. Journal of cellular physiology, 2019; 234(4): 4515-4527.
16. Logotheti S, Marquardt S, Gupta S, Richter C, Edelhäuser B, Engelmann D, et al. LncRNA-SLC16A1-AS1 induces metabolic reprogramming during Bladder Cancer progression as target and co-activator of E2F1. Theranostics, 2020; 10(21): 9620-9643.
17. Ma X, Li B, Liu J, Fu Y, and Luo Y. Phosphoglycerate dehydrogenase promotes pancreatic cancer development by interacting with eIF4A1 and eIF4E. Journal of experimental & clinical cancer research : CR, 2019; 38(1): 66.
18. Fan C, Tang Y, Wang J, Xiong F, Guo C, Wang Y, et al. Role of long non-coding RNAs in glucose metabolism in cancer. Molecular cancer, 2017; 16(1): 130.
19. Liu J, Liu Z, Wu Q, Lu Y, Wong C, Miao L, et al. Long noncoding RNA AGPG regulates PFKFB3-mediated tumor glycolytic reprogramming. Nature communications, 2020; 11(1): 1507.
20. Zhao Y, Liu Y, Lin L, Huang Q, He W, Zhang S, et al. The lncRNA MACC1-AS1 promotes gastric cancer cell metabolic plasticity via AMPK/Lin28 mediated mRNA stability of MACC1. Molecular cancer, 2018; 17(1): 69.
21. Peng F, Wang J, Fan W, Meng Y, Li M, Li T, et al. Glycolysis gatekeeper PDK1 reprograms breast cancer stem cells under hypoxia. Oncogene, 2018; 37(8): 1062-1074.
22. Hesketh R, Wang J, Wright A, Lewis D, Denton A, Grenfell R, et al. Magnetic Resonance Imaging Is More Sensitive Than PET for Detecting Treatment-Induced Cell Death-Dependent Changes in Glycolysis. Cancer research, 2019; 79(14): 3557-3569.
23. Gottfried E, Kreutz M, and Mackensen A. Tumor metabolism as modulator of immune response and tumor progression. Seminars in cancer biology, 2012; 22(4): 335-41.
24. Ippolito L, Morandi A, Giannoni E, and Chiarugi P. Lactate: A Metabolic Driver in the Tumour Landscape. Trends in biochemical sciences, 2019; 44(2): 153-166.
25. Brand A, Singer K, Koehl G, Kolitzus M, Schoenhammer G, Thiel A, et al. LDHA-Associated Lactic Acid Production Blunts Tumor Immunosurveillance by T and NK Cells. Cell metabolism, 2016; 24(5): 657-671.
26. Wang R, Ma Y, Zhan S, Zhang G, Cao L, Zhang X, et al. B7-H3 promotes colorectal cancer angiogenesis through activating the NF-κB pathway to induce VEGFA expression. Cell death & disease, 2020; 11(1): 55.
27. Zhong Q, Fang Y, Lai Q, Wang S, He C, Li A, et al. CPEB3 inhibits epithelial-mesenchymal transition by disrupting the crosstalk between colorectal cancer cells and tumor-associated macrophages via IL-6R/STAT3 signaling. Journal of experimental & clinical cancer research : CR, 2020; 39(1): 132.
28. Shi T, Ma Y, Cao L, Zhan S, Xu Y, Fu F, et al. B7-H3 promotes aerobic glycolysis and chemoresistance in colorectal cancer cells by regulating HK2. Cell death & disease, 2019; 10(4): 308.
29. Lu H, Shi T, Wang M, Li X, Gu Y, Zhang X, et al. B7-H3 inhibits the IFN-γ-dependent cytotoxicity of Vγ9Vδ2 T cells against colon cancer cells. Oncoimmunology, 2020; 9(1): 1748991.

30. Zheng X, Zhou Y, Chen W, Chen L, Lu J, He F, et al. Ginsenoside 20(S)-Rg3 Prevents PKM2-Targeting miR-324-5p from H19 Sponging to Antagonize the Warburg Effect in Ovarian Cancer Cells. Cellular physiology and biochemistry : international journal of experimental cellular physiology, biochemistry, and pharmacology, 2018; 51(3): 1340-1353.
31. Wu Z, Yan L, Liu Y, Cao L, Guo Y, Zhang Y, et al. Inhibition of mTORC1 by lncRNA H19 via disrupting 4E-BP1/Raptor interaction in pituitary tumours. Nature communications, 2018; 9(1): 4624.
32. Wang S, Ma F, Tang Z, Wu X, Cai Q, Zhang M, et al. Long non-coding RNA H19 regulates FOXM1 expression by competitively binding endogenous miR-342-3p in gallbladder cancer. Journal of experimental & clinical cancer research : CR, 2016; 35(1): 160.
33. Vennin C, Spruyt N, Robin Y, Chassat T, Le Bourhis X, and Adriaenssens E. The long non-coding RNA 91H increases aggressive phenotype of breast cancer cells and up-regulates H19/IGF2 expression through epigenetic modifications. Cancer letters, 2017; 385: 198-206.
34. Husain Z, Huang Y, Seth P, and Sukhatme V. Tumor-derived lactate modifies antitumor immune response: effect on myeloid-derived suppressor cells and NK cells. Journal of immunology (Baltimore, Md. : 1950), 2013; 191(3): 1486-95.
35. Thelen F and Witherden D. Get in Touch With Dendritic Epithelial T Cells! Frontiers in immunology, 2020; 11: 1656.
36. Gan L, Lv L, and Liao S. Long non-coding RNA H19 regulates cell growth and metastasis via the miR-22-3p/Snail1 axis in gastric cancer. International journal of oncology, 2019; 54(6): 2157-2168.
37. Liu G, Xiang T, Wu Q, and Wang W. Long Noncoding RNA H19-Derived miR-675 Enhances Proliferation and Invasion via RUNX1 in Gastric Cancer Cells. Oncology research, 2016; 23(3): 99-107.
38. Li X, Zhang C, Zhao T, Su Z, Li M, Hu J, et al. Lysine-222 succinylation reduces lysosomal degradation of lactate dehydrogenase a and is increased in gastric cancer. Journal of experimental & clinical cancer research : CR, 2020; 39(1): 172.
39. Zhu W, Ma L, Qian J, Xu J, Xu T, Pang L, et al. The molecular mechanism and clinical significance of LDHA in HER2-mediated progression of gastric cancer. American journal of translational research, 2018; 10(7): 2055-2067.
40. Wang H, Zhou R, Sun L, Xia J, Yang X, Pan C, et al. TOP1MT deficiency promotes GC invasion and migration via the enhancements of LDHA expression and aerobic glycolysis. Endocrine-related cancer, 2017; 24(11): 565-578.
41. Wei C and Gao J. Downregulated miR-383-5p contributes to the proliferation and migration of gastric cancer cells and is associated with poor prognosis. PeerJ, 2019; 7: e7882.
42. Liang Y, Song X, Li Y, Chen B, Zhao W, Wang L, et al. LncRNA BCRT1 promotes breast cancer progression by targeting miR-1303/PTBP3 axis. Molecular cancer, 2020; 19(1): 85.
43. Tang X, Sun G, He Q, Wang C, Shi J, Gao L, et al. Circular noncoding RNA circMBOAT2 is a novel tumor marker and regulates proliferation/migration by sponging miR-519d-3p in colorectal cancer. Cell death & disease, 2020; 11(8): 625.

44. Li D, Song H, Wu T, Xie D, Hu J, Zhao J, et al. MiR-519d-3p suppresses breast cancer cell growth and motility via targeting LIM domain kinase 1. Molecular and cellular biochemistry, 2018; 444: 169-178.
45. Sun J, Zhang P, Yin T, Zhang F, and Wang W. Upregulation of LncRNA PVT1 Facilitates Pancreatic Ductal Adenocarcinoma Cell Progression and Glycolysis by Regulating MiR-519d-3p and HIF-1A. Journal of Cancer, 2020; 11(9): 2572-2579.
46. Li Y, Shao J, Zhang S, Xing G, and Liu H. miR-519d-3p Inhibits Cell Proliferation and Invasion of Gastric Cancer by Downregulating B-Cell Lymphoma 6. Cytogenetic and genome research, 2018; 154(1): 12-19.
47. Chen P, Zuo H, Xiong H, Kolar M, Chu Q, Saghatelian A, et al. Gpr132 sensing of lactate mediates tumor-macrophage interplay to promote breast cancer metastasis. Proceedings of the National Academy of Sciences of the United States of America, 2017; 114(3): 580-585.
48. Ping W, Senyan H, Li G, Yan C, and Long L. Increased Lactate in Gastric Cancer Tumor-Infiltrating Lymphocytes Is Related to Impaired T Cell Function Due to miR-34a Deregulated Lactate Dehydrogenase A. Cellular physiology and biochemistry : international journal of experimental cellular physiology, biochemistry, and pharmacology, 2018; 49(2): 828-836.
49. Benyamine A, Le Roy A, Mamessier E, Gertner-Dardenne J, Castanier C, Orlanducci F, et al. BTN3A molecules considerably improve Vγ9Vδ2T cells-based immunotherapy in acute myeloid leukemia. Oncoimmunology, 2016; 5(10): e1146843.
50. Wang J, Lin C, Li H, Li R, Wu Y, Liu H, et al. Tumor-infiltrating γδT cells predict prognosis and adjuvant chemotherapeutic benefit in patients with gastric cancer. Oncoimmunology, 2017; 6(11): e1353858.

Figures

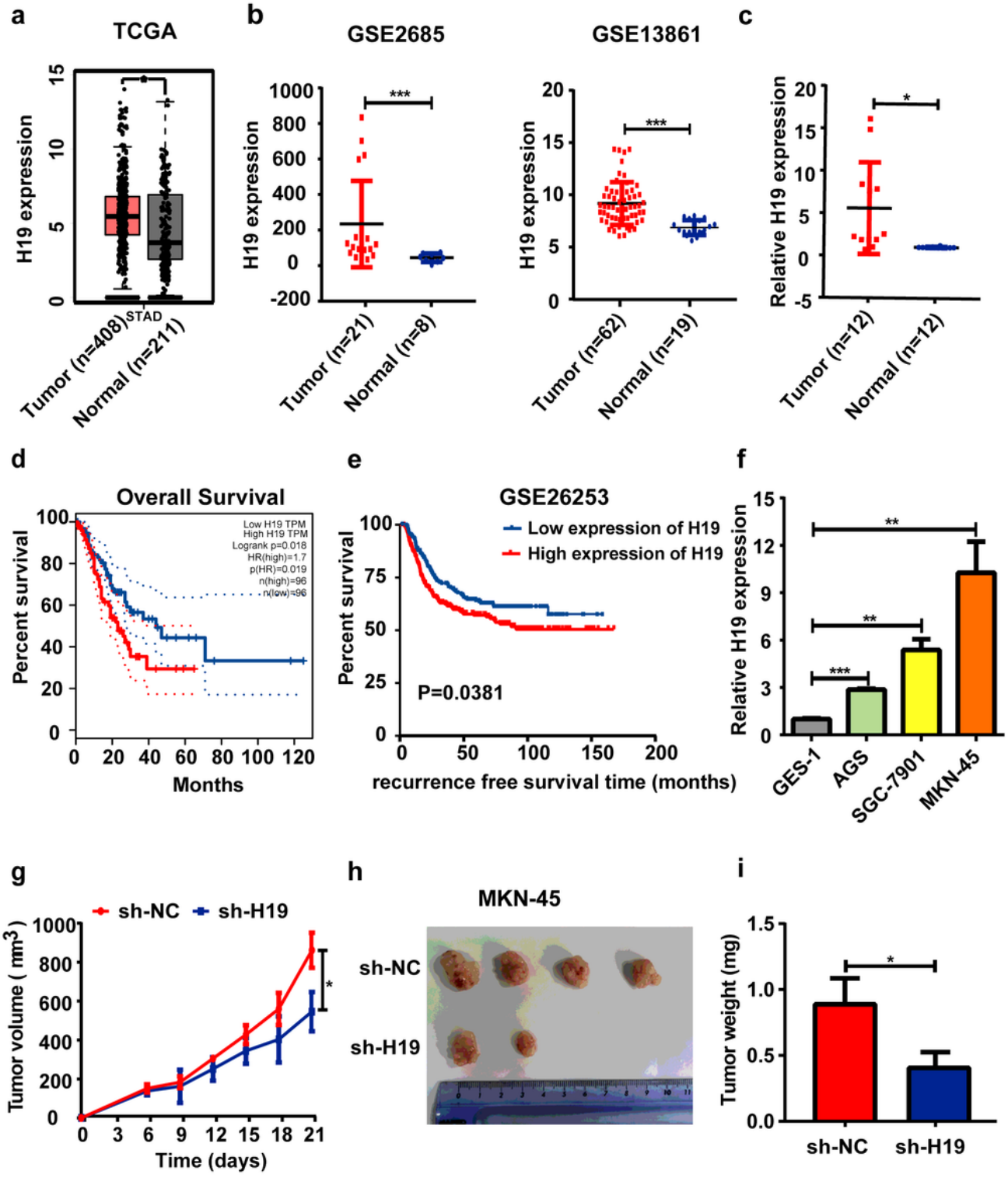

Figure 1

H19 was overexpression in GC tissue specimens and promoted tumor growth in vivo. a Expression of H19 in GC tissue samples from TCGA data based on GEPIA. b Expression of H19 from two microarray datasets (GSE2685 and GSE13861). c Expression of H19 in 12 pairs of GC and adjacent normal tissue specimens. d The relationship between the expression of H19 and the overall survival of GC patients from TCGA data based on GEPIA. e The relationship between the expression of H19 and the recurrence-free

survival of GC patients from GSE26253 database. f Expression of H19 in GES-1, AGS, SGC-7901, and MKN-45 cells. g-i Tumor volume (g), image (h), and weight (i) of H19 knockdown MKN-45 tumors in nude mice. n=4 mice per group. Each experiment was performed in triplicate. Data are presented as the mean ± SD and analyzed by student's t-test (*p<0.05, **p<0.01, ***p<0.001)

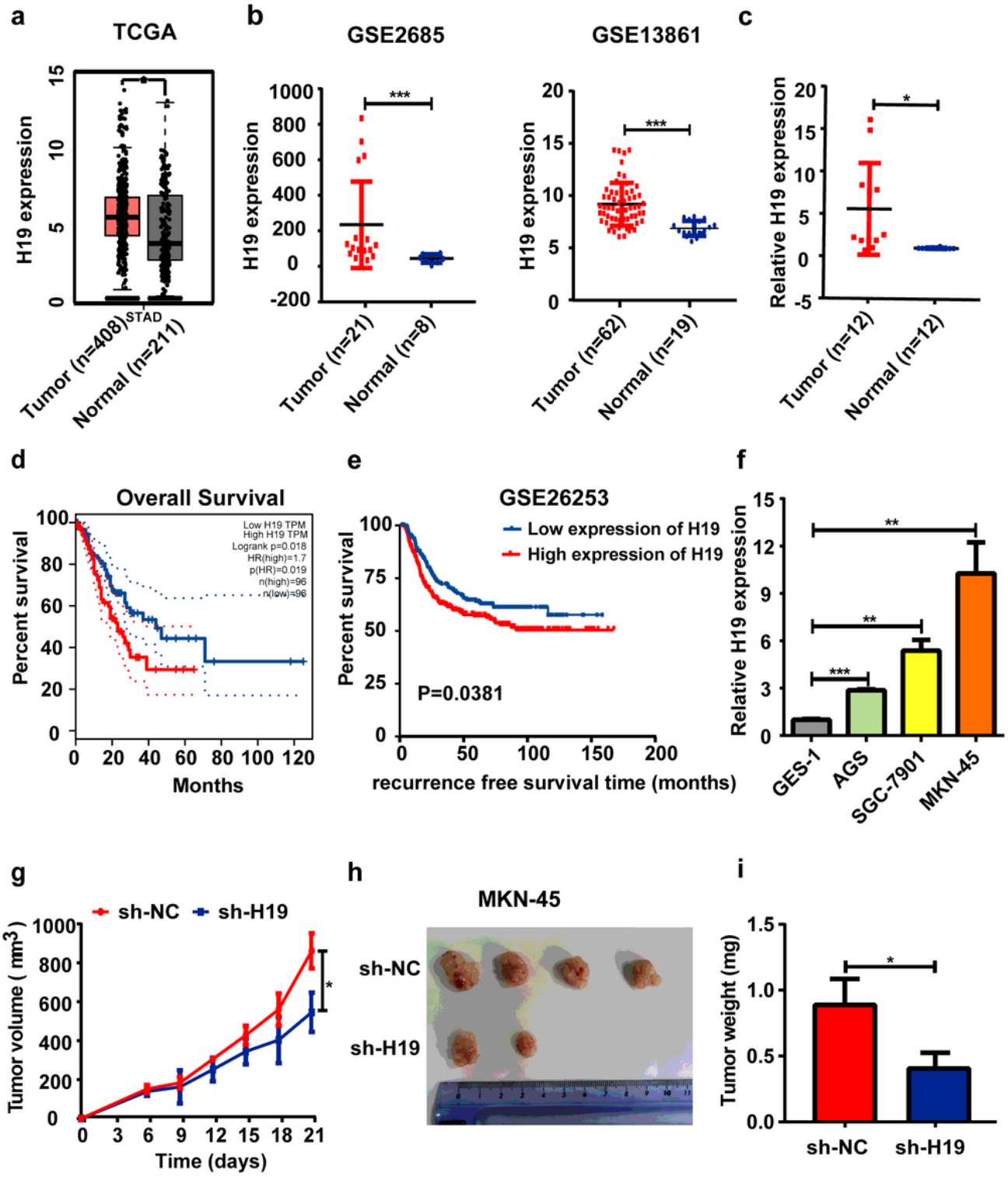

Figure 1

H19 was overexpression in GC tissue specimens and promoted tumor growth in vivo. a Expression of H19 in GC tissue samples from TCGA data based on GEPIA. b Expression of H19 from two microarray datasets (GSE2685 and GSE13861). c Expression of H19 in 12 pairs of GC and adjacent normal tissue specimens. d The relationship between the expression of H19 and the overall survival of GC patients from TCGA data based on GEPIA. e The relationship between the expression of H19 and the recurrence-free survival of GC patients from GSE26253 database. f Expression of H19 in GES-1, AGS, SGC-7901, and MKN-45 cells. g-i Tumor volume (g), image (h), and weight (i) of H19 knockdown MKN-45 tumors in nude mice. n=4 mice per group. Each experiment was performed in triplicate. Data are presented as the mean ± SD and analyzed by student's t-test (*$p<0.05$, **$p<0.01$, ***$p<0.001$)

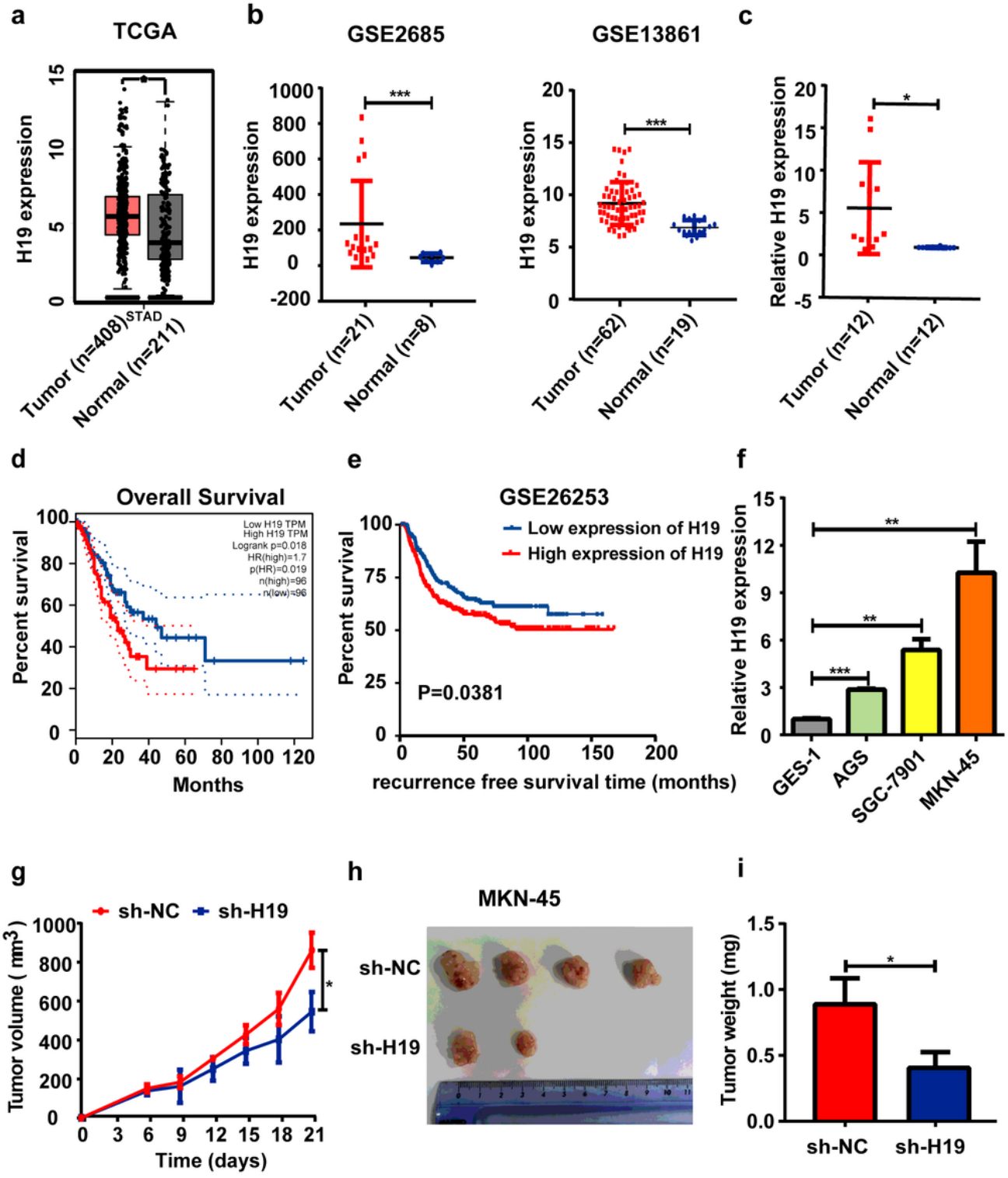

Figure 1

H19 was overexpression in GC tissue specimens and promoted tumor growth in vivo. a Expression of H19 in GC tissue samples from TCGA data based on GEPIA. b Expression of H19 from two microarray datasets (GSE2685 and GSE13861). c Expression of H19 in 12 pairs of GC and adjacent normal tissue specimens. d The relationship between the expression of H19 and the overall survival of GC patients from TCGA data based on GEPIA. e The relationship between the expression of H19 and the recurrence-free

survival of GC patients from GSE26253 database. f Expression of H19 in GES-1, AGS, SGC-7901, and MKN-45 cells. g-i Tumor volume (g), image (h), and weight (i) of H19 knockdown MKN-45 tumors in nude mice. n=4 mice per group. Each experiment was performed in triplicate. Data are presented as the mean ± SD and analyzed by student's t-test (*p<0.05, **p<0.01, ***p<0.001)

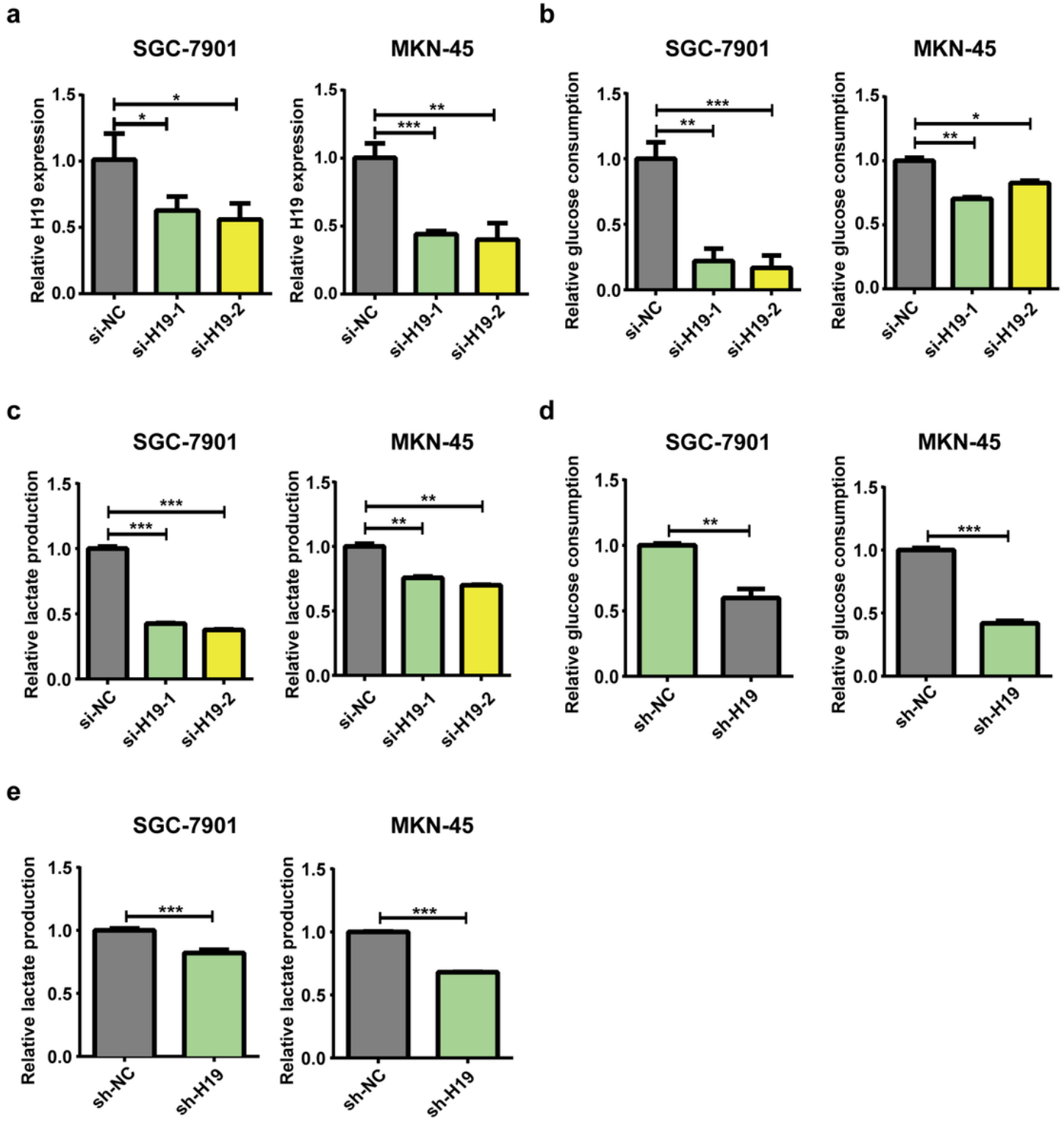

Figure 2

H19 knockdown inhibited aerobic glycolysis in GC cells. a H19 levels in SGC-7901 and MKN-45 cells were analyzed by RT-qPCR after transfection with siRNA negative control (si-NC), H19 siRNA-1 (si-H19-1) or H19 siRNA-2 (si-H19-2). b-c Glucose consumption (b) and lactate production (c) were measured in SGC-7901 and MKN-45 cells after transfection with si-NC, si-H19-1, or si-H19-2. d-e Glucose consumption (d) and lactate production (e) were measured in both stable knockdown H19 (sh-H19) SGC-7901 and MKN-45 cells. Each experiment was performed in triplicate. Data are presented as the mean ± SD and analyzed by student's t-test (*p<0.05, **p<0.01, ***p<0.001)

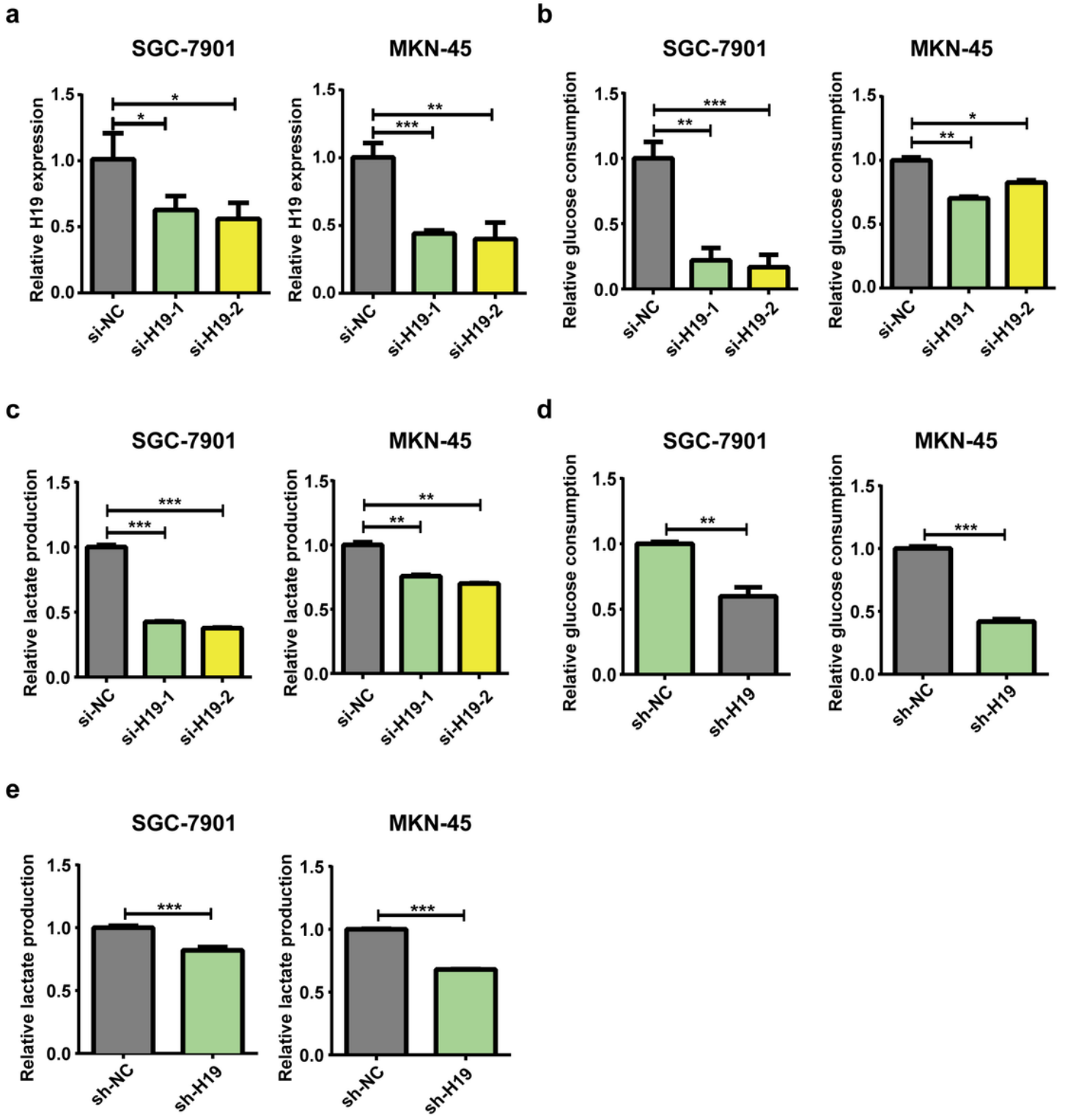

Figure 2

H19 knockdown inhibited aerobic glycolysis in GC cells. a H19 levels in SGC-7901 and MKN-45 cells were analyzed by RT-qPCR after transfection with siRNA negative control (si-NC), H19 siRNA-1 (si-H19-1) or H19 siRNA-2 (si-H19-2). b-c Glucose consumption (b) and lactate production (c) were measured in SGC-7901 and MKN-45 cells after transfection with si-NC, si-H19-1, or si-H19-2. d-e Glucose consumption (d) and lactate production (e) were measured in both stable knockdown H19 (sh-H19) SGC-7901 and MKN-45 cells. Each experiment was performed in triplicate. Data are presented as the mean ± SD and analyzed by student's t-test (*$p<0.05$, **$p<0.01$, ***$p<0.001$)

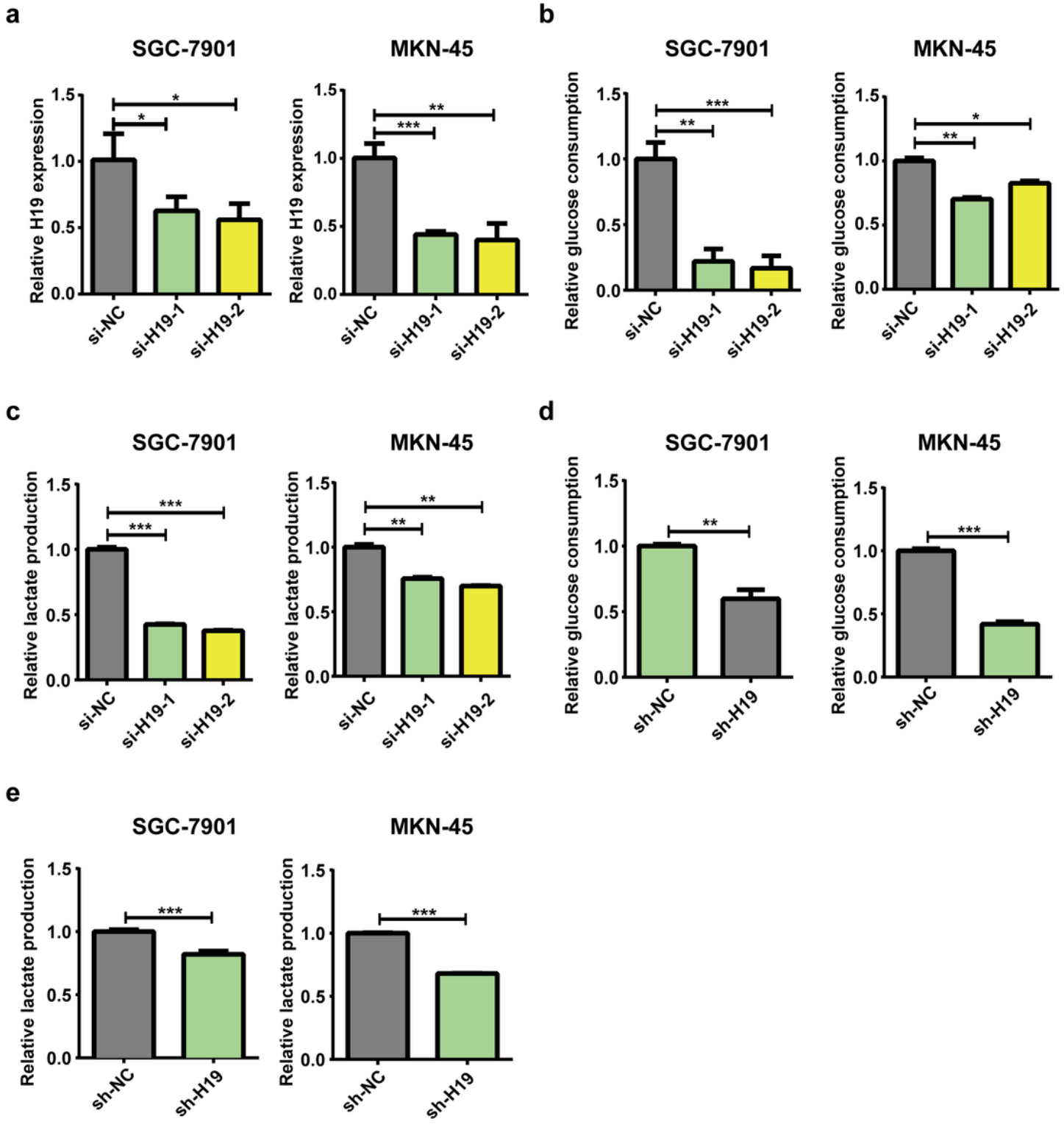

Figure 2

H19 knockdown inhibited aerobic glycolysis in GC cells. a H19 levels in SGC-7901 and MKN-45 cells were analyzed by RT-qPCR after transfection with siRNA negative control (si-NC), H19 siRNA-1 (si-H19-1) or H19 siRNA-2 (si-H19-2). b-c Glucose consumption (b) and lactate production (c) were measured in SGC-7901 and MKN-45 cells after transfection with si-NC, si-H19-1, or si-H19-2. d-e Glucose consumption (d) and lactate production (e) were measured in both stable knockdown H19 (sh-H19) SGC-7901 and MKN-

45 cells. Each experiment was performed in triplicate. Data are presented as the mean ± SD and analyzed by student's t-test (*p<0.05, **p<0.01, ***p<0.001)

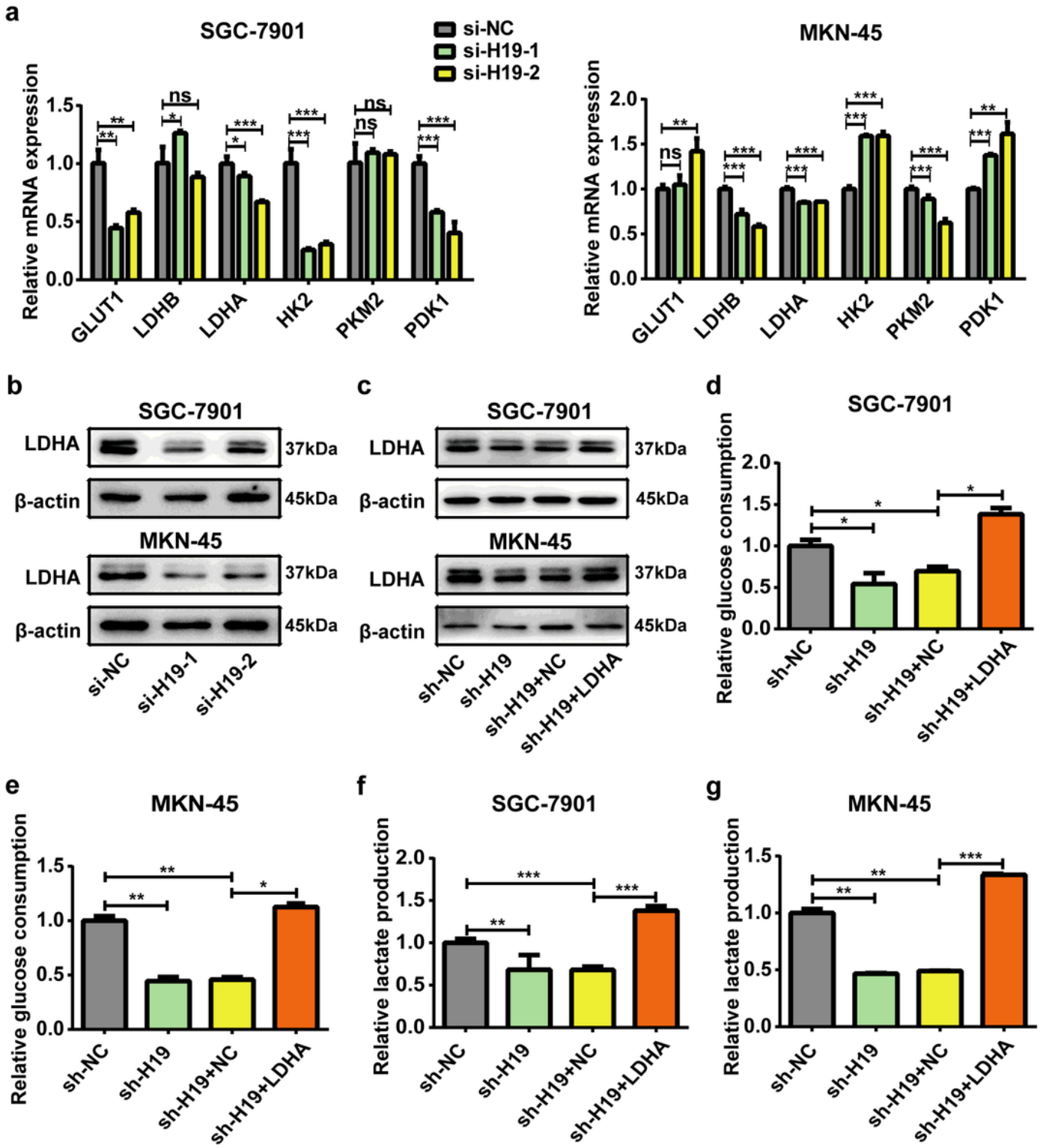

Figure 3

H19 knockdown inhibited aerobic glycolysis through LDHA. a The expression of glycolysis-related genes were examined by RT-qPCR in SGC-7901 and MKN-45 cells after transfection with si-NC, si-H19-1, or si-H19-2. b LDHA protein level was detected by western blot in SGC-7901 and MKN-45 cells after

transfection with si-NC, si-H19-1, or si-H19-2. β-actin served as a loading control. c LDHA protein level was detected by western blot in both stable knockdown H19 (sh-H19) SGC-7901 and MKN-45 cells after transfection with negative control plasmid (NC) or LDHA overexpression plasmid (LDHA). β-actin served as a loading control. d-g Glucose consumption (d, e) and lactate production (f, g) were examined in both sh-H19 SGC-7901 and MKN-45 cells after transfection with NC or LDHA. Each experiment was performed in triplicate. Data are presented as the mean ± SD and analyzed by student's t-test (*p<0.05, **p<0.01, ***p<0.001, ns. not significant)

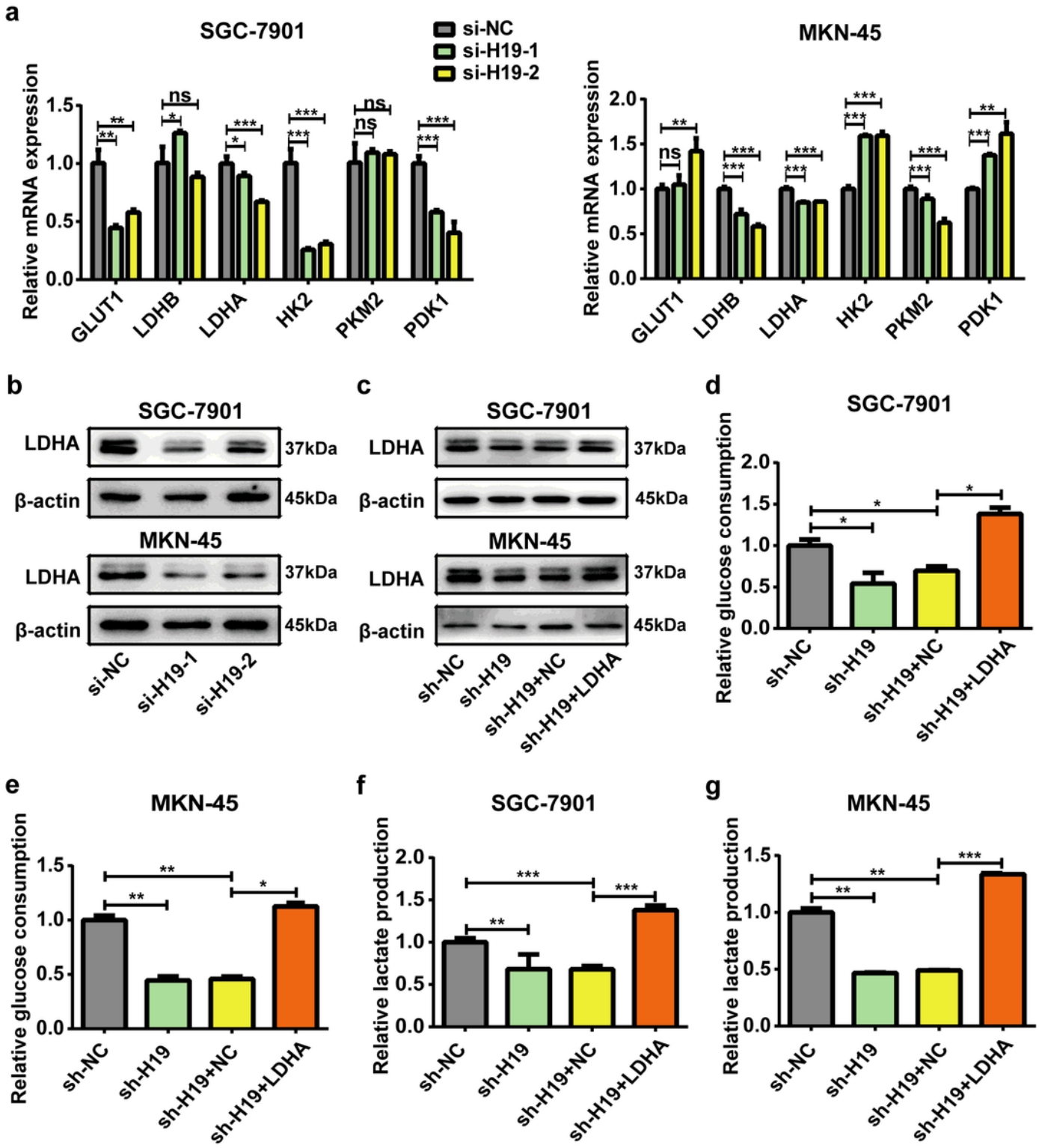

Figure 3

H19 knockdown inhibited aerobic glycolysis through LDHA. a The expression of glycolysis-related genes were examined by RT-qPCR in SGC-7901 and MKN-45 cells after transfection with si-NC, si-H19-1, or si-H19-2. b LDHA protein level was detected by western blot in SGC-7901 and MKN-45 cells after transfection with si-NC, si-H19-1, or si-H19-2. β-actin served as a loading control. c LDHA protein level was detected by western blot in both stable knockdown H19 (sh-H19) SGC-7901 and MKN-45 cells after transfection with negative control plasmid (NC) or LDHA overexpression plasmid (LDHA). β-actin served as a loading control. d-g Glucose consumption (d, e) and lactate production (f, g) were examined in both sh-H19 SGC-7901 and MKN-45 cells after transfection with NC or LDHA. Each experiment was performed in triplicate. Data are presented as the mean ± SD and analyzed by student's t-test (*p<0.05, **p<0.01, ***p<0.001, ns. not significant)

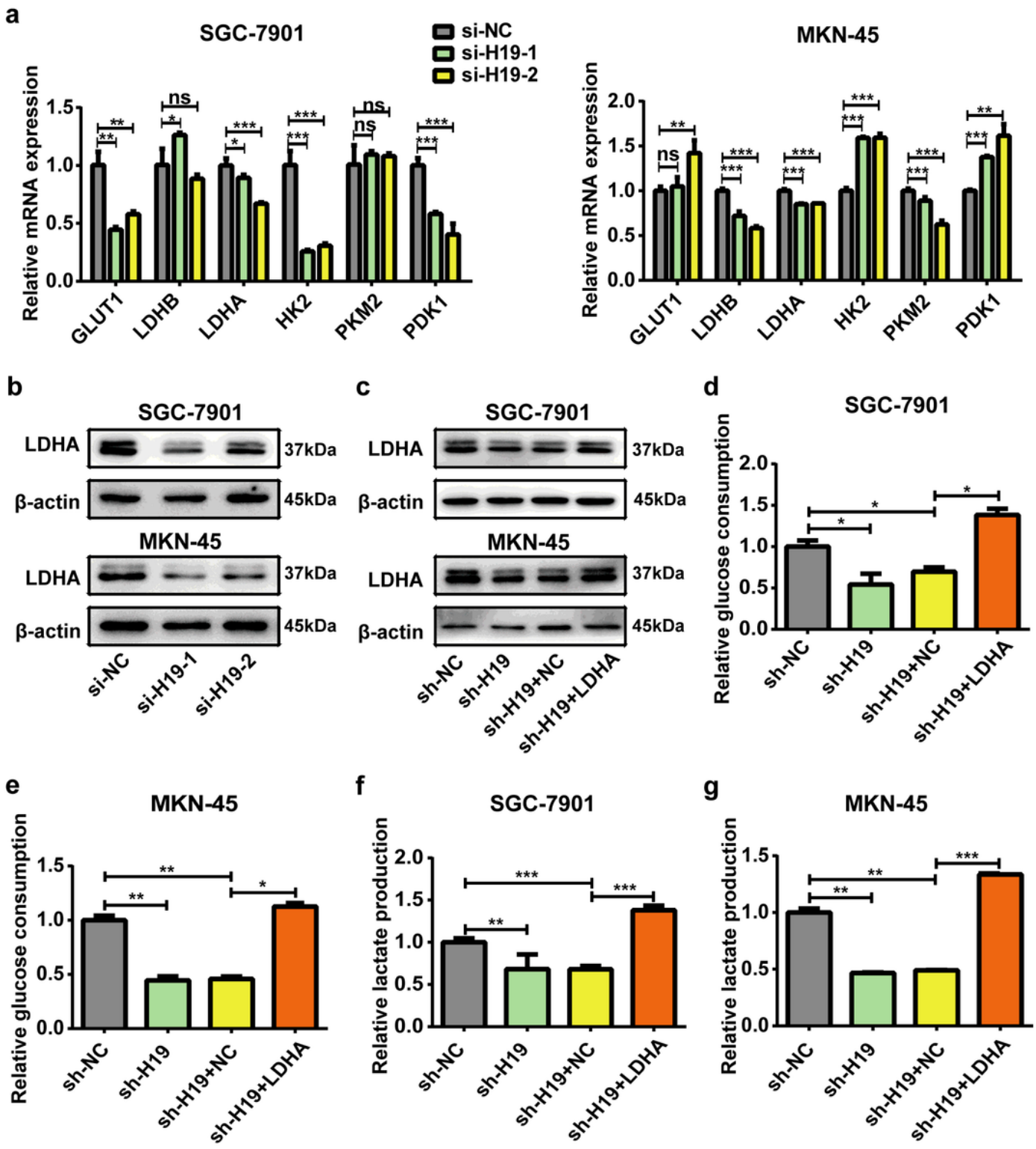

Figure 3

H19 knockdown inhibited aerobic glycolysis through LDHA. a The expression of glycolysis-related genes were examined by RT-qPCR in SGC-7901 and MKN-45 cells after transfection with si-NC, si-H19-1, or si-H19-2. b LDHA protein level was detected by western blot in SGC-7901 and MKN-45 cells after transfection with si-NC, si-H19-1, or si-H19-2. β-actin served as a loading control. c LDHA protein level was detected by western blot in both stable knockdown H19 (sh-H19) SGC-7901 and MKN-45 cells after

transfection with negative control plasmid (NC) or LDHA overexpression plasmid (LDHA). β-actin served as a loading control. d-g Glucose consumption (d, e) and lactate production (f, g) were examined in both sh-H19 SGC-7901 and MKN-45 cells after transfection with NC or LDHA. Each experiment was performed in triplicate. Data are presented as the mean ± SD and analyzed by student's t-test (*p<0.05, **p<0.01, ***p<0.001, ns. not significant)

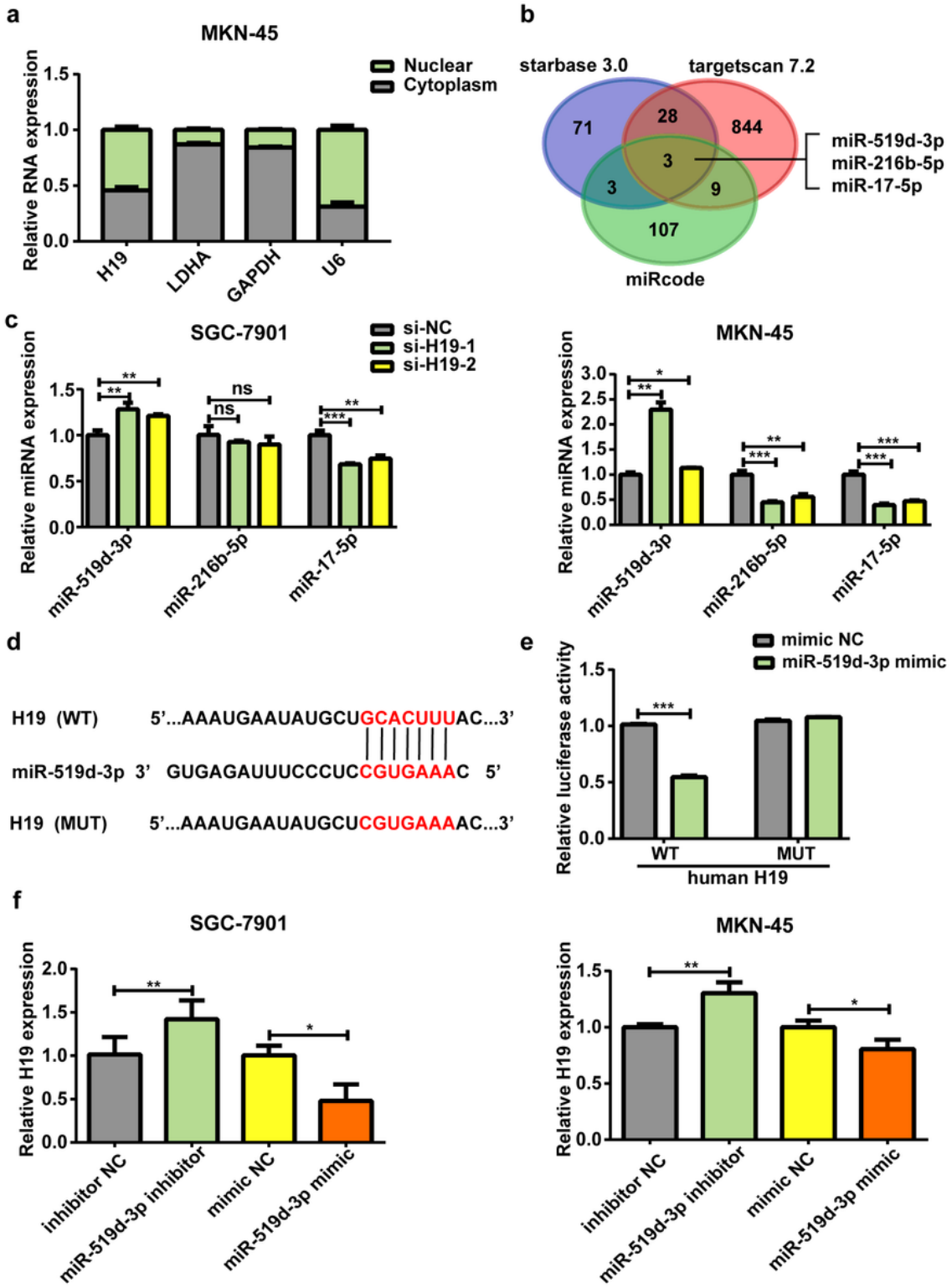

Figure 4

H19 sponged miR-519d-3p in GC cells. a The subcellular distribution of H19 and LDHA was examined by nuclear and cytoplasmic separation experiments with RT-qPCR in MKN-45 cells. b Three putative miRNAs targeting both H19 and LDHA were predicted by three different algorithms (starbase3.0 for H19, targetscan7.2 for LDHA, and miRcode for H19). c The levels of miR-519d-3p, miR-216b-5p, and miR-17-5p were detected by RT-qPCR in SGC-7901 and MKN-45 cells after transfection with si-NC, si-H19-1 or si-H19-2. d The hybridization models between H19 and miR-519d-3p. e Luciferase reporter assay showed the binding of miR-519d-3p and wide type (WT) H19 but not mutant (MUT) H19. f The mRNA levels of H19 were measured by RT-qPCR in both SGC-7901 and MKN-45 cells after transfection with inhibitor negative control (NC), miR-519d-3p inhibitor, mimic NC, or miR-519d-3p mimic. Each experiment was performed in triplicate. Data are presented as the mean ± SD and analyzed by student's t-test (*p<0.05, **p<0.01, ***p<0.001, ns. not significant)

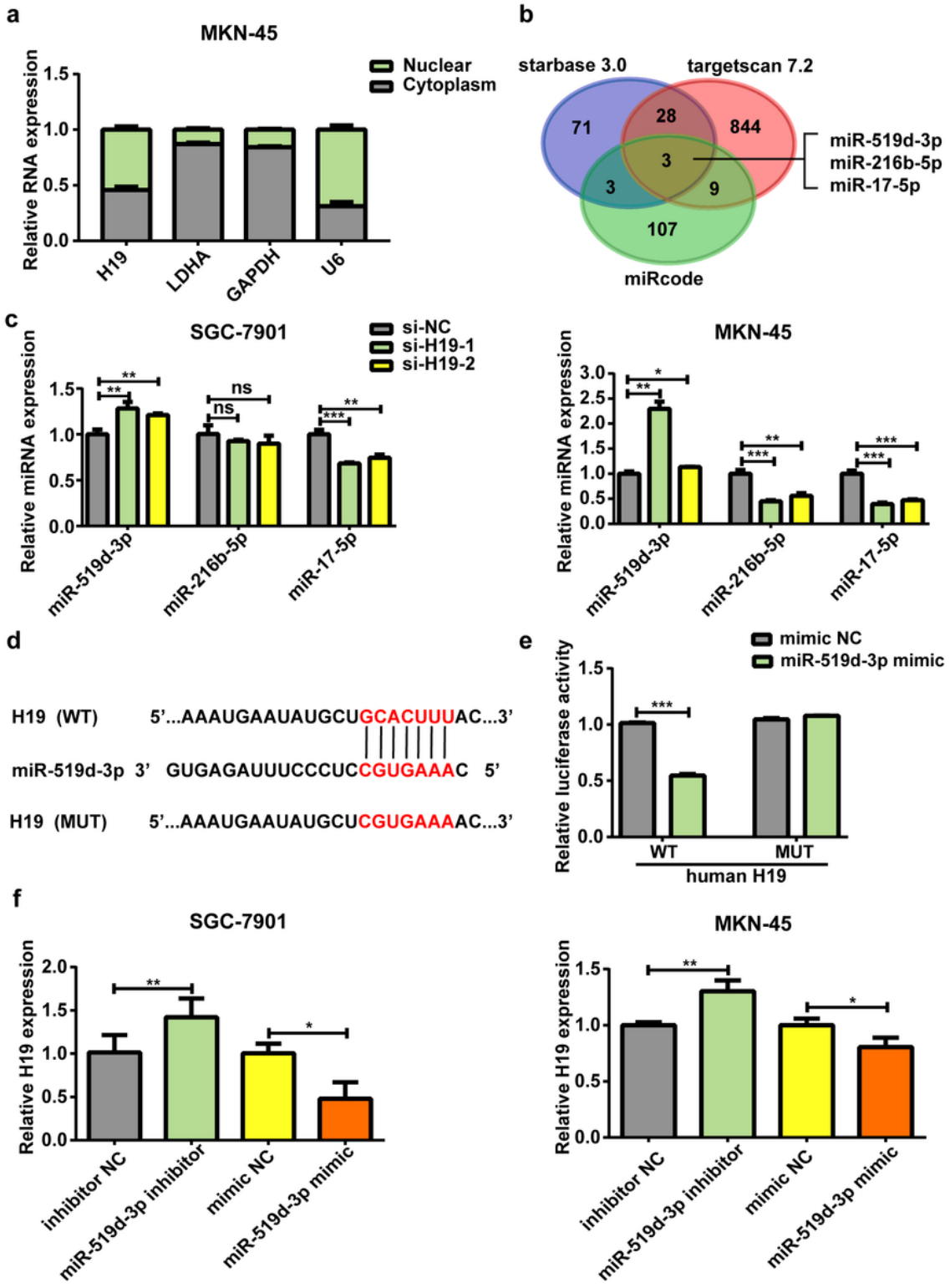

Figure 4

H19 sponged miR-519d-3p in GC cells. a The subcellular distribution of H19 and LDHA was examined by nuclear and cytoplasmic separation experiments with RT-qPCR in MKN-45 cells. b Three putative miRNAs targeting both H19 and LDHA were predicted by three different algorithms (starbase3.0 for H19, targetscan7.2 for LDHA, and miRcode for H19). c The levels of miR-519d-3p, miR-216b-5p, and miR-17-5p were detected by RT-qPCR in SGC-7901 and MKN-45 cells after transfection with si-NC, si-H19-1 or si-H19-

2. d The hybridization models between H19 and miR-519d-3p. e Luciferase reporter assay showed the binding of miR-519d-3p and wide type (WT) H19 but not mutant (MUT) H19. f The mRNA levels of H19 were measured by RT-qPCR in both SGC-7901 and MKN-45 cells after transfection with inhibitor negative control (NC), miR-519d-3p inhibitor, mimic NC, or miR-519d-3p mimic. Each experiment was performed in triplicate. Data are presented as the mean ± SD and analyzed by student's t-test (*p<0.05, **p<0.01, ***p<0.001, ns. not significant)

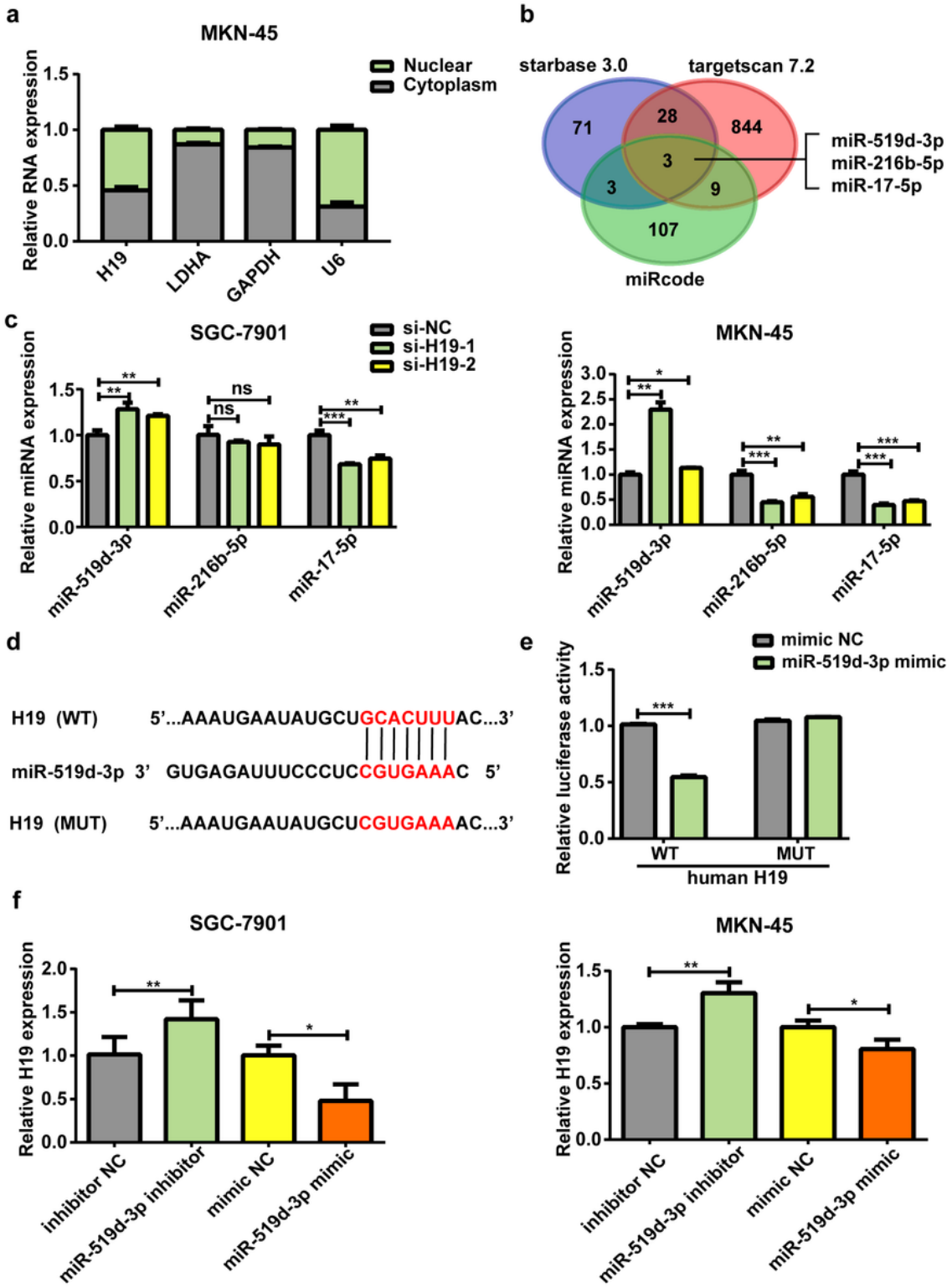

Figure 4

H19 sponged miR-519d-3p in GC cells. a The subcellular distribution of H19 and LDHA was examined by nuclear and cytoplasmic separation experiments with RT-qPCR in MKN-45 cells. b Three putative miRNAs targeting both H19 and LDHA were predicted by three different algorithms (starbase3.0 for H19, targetscan7.2 for LDHA, and miRcode for H19). c The levels of miR-519d-3p, miR-216b-5p, and miR-17-5p were detected by RT-qPCR in SGC-7901 and MKN-45 cells after transfection with si-NC, si-H19-1 or si-H19-2. d The hybridization models between H19 and miR-519d-3p. e Luciferase reporter assay showed the binding of miR-519d-3p and wide type (WT) H19 but not mutant (MUT) H19. f The mRNA levels of H19 were measured by RT-qPCR in both SGC-7901 and MKN-45 cells after transfection with inhibitor negative control (NC), miR-519d-3p inhibitor, mimic NC, or miR-519d-3p mimic. Each experiment was performed in triplicate. Data are presented as the mean ± SD and analyzed by student's t-test (*p<0.05, **p<0.01, ***p<0.001, ns. not significant)

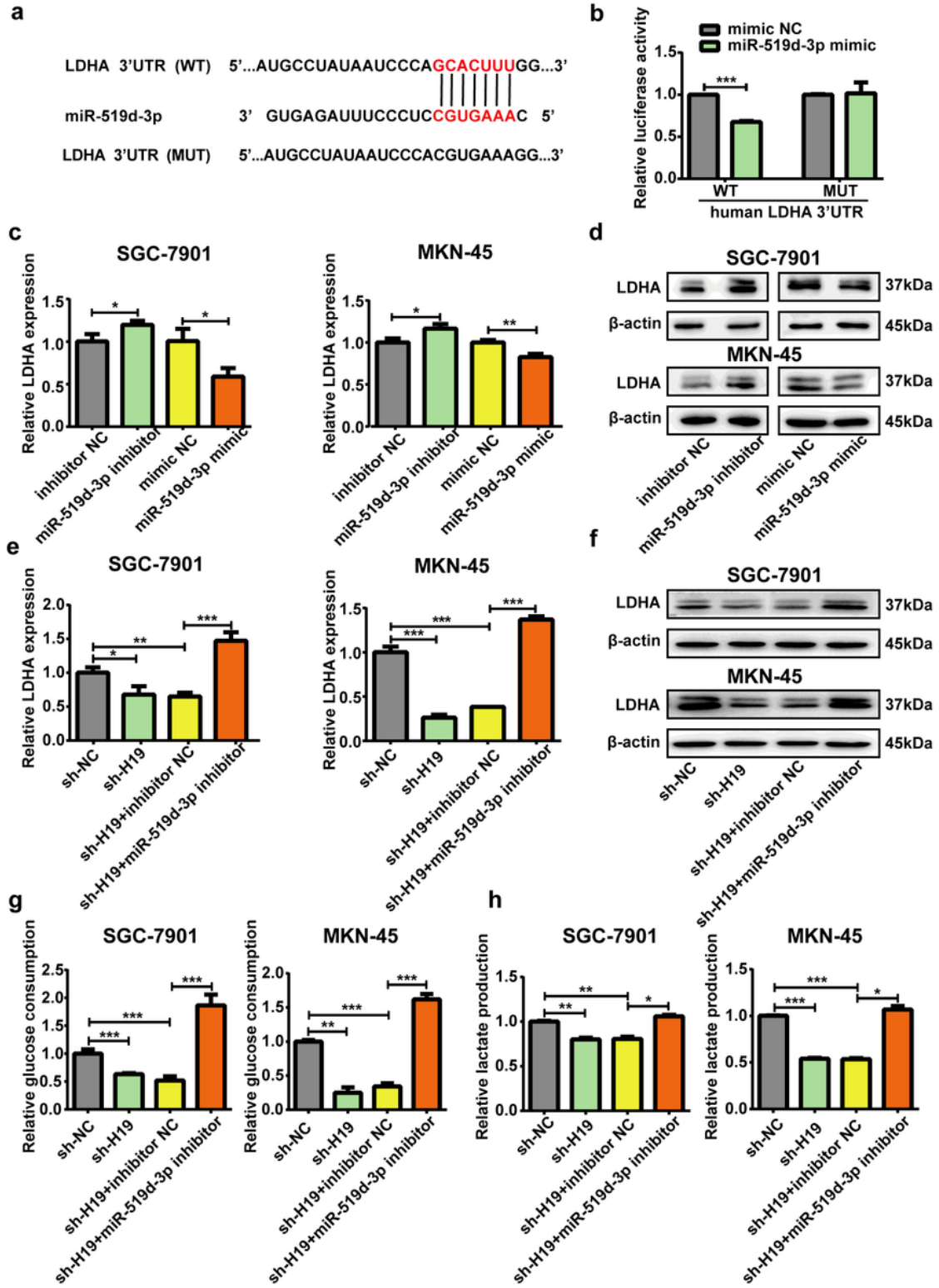

Figure 5

H19 regulated LDHA expression and glycolysis via miR-519d-3p. a The hybridization models between LDHA and miR-519d-3p. b Luciferase reporter assay showed the binding of miR-519d-3p and wide type (WT) LDHA 3'UTR but not mutant (MUT) LDHA 3'UTR. c-d The mRNA (c) and protein (d) levels of LDHA were measured in both SGC-7901 and MKN-45 cells after transfection with inhibitor negative control (NC), miR-519d-3p inhibitor, mimic NC, or miR-519d-3p mimic. β-actin served as a loading control. e-f The

mRNA (e) and protein (f) levels of LDHA were measured in both sh-H19 SGC-7901 and MKN-45 cells after transfection with inhibitor NC or miR-519d-3p inhibitor. β-actin served as a loading control. g-h Glucose consumption (g) and lactate production (h) were examined in both sh-H19 SGC-7901 and MKN-45 cells after transfection with inhibitor NC or miR-519d-3p inhibitor. Each experiment was performed in triplicate. Data are presented as the mean ± SD and analyzed by student's t-test (*p<0.05, **p<0.01, ***p<0.001)

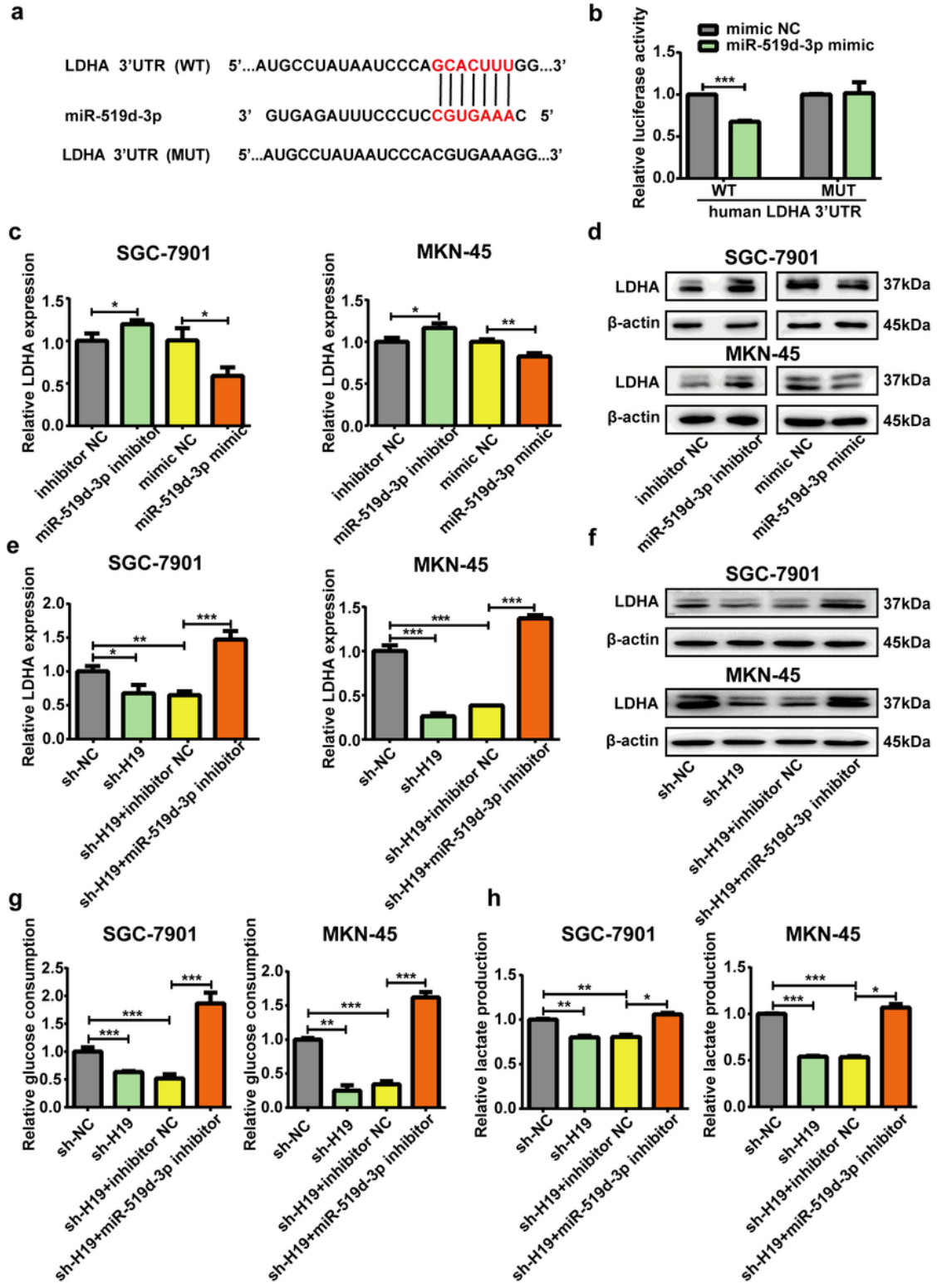

Figure 5

H19 regulated LDHA expression and glycolysis via miR-519d-3p. a The hybridization models between LDHA and miR-519d-3p. b Luciferase reporter assay showed the binding of miR-519d-3p and wide type (WT) LDHA 3'UTR but not mutant (MUT) LDHA 3'UTR. c-d The mRNA (c) and protein (d) levels of LDHA were measured in both SGC-7901 and MKN-45 cells after transfection with inhibitor negative control (NC), miR-519d-3p inhibitor, mimic NC, or miR-519d-3p mimic. β-actin served as a loading control. e-f The mRNA (e) and protein (f) levels of LDHA were measured in both sh-H19 SGC-7901 and MKN-45 cells after transfection with inhibitor NC or miR-519d-3p inhibitor. β-actin served as a loading control. g-h Glucose consumption (g) and lactate production (h) were examined in both sh-H19 SGC-7901 and MKN-45 cells after transfection with inhibitor NC or miR-519d-3p inhibitor. Each experiment was performed in triplicate. Data are presented as the mean ± SD and analyzed by student's t-test (*$p<0.05$, **$p<0.01$, ***$p<0.001$)

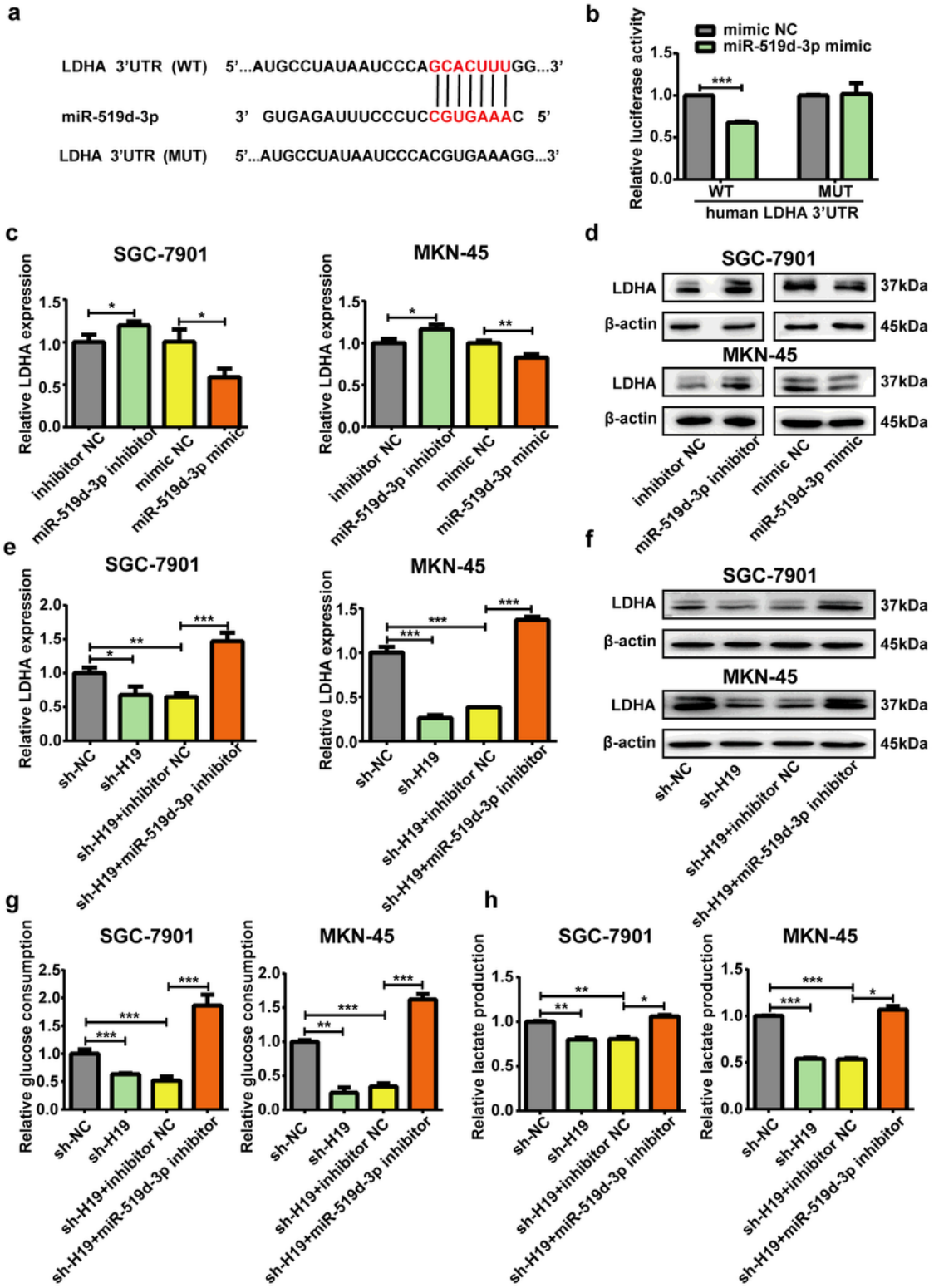

Figure 5

H19 regulated LDHA expression and glycolysis via miR-519d-3p. a The hybridization models between LDHA and miR-519d-3p. b Luciferase reporter assay showed the binding of miR-519d-3p and wide type (WT) LDHA 3'UTR but not mutant (MUT) LDHA 3'UTR. c-d The mRNA (c) and protein (d) levels of LDHA were measured in both SGC-7901 and MKN-45 cells after transfection with inhibitor negative control (NC), miR-519d-3p inhibitor, mimic NC, or miR-519d-3p mimic. β-actin served as a loading control. e-f The

mRNA (e) and protein (f) levels of LDHA were measured in both sh-H19 SGC-7901 and MKN-45 cells after transfection with inhibitor NC or miR-519d-3p inhibitor. β-actin served as a loading control. g-h Glucose consumption (g) and lactate production (h) were examined in both sh-H19 SGC-7901 and MKN-45 cells after transfection with inhibitor NC or miR-519d-3p inhibitor. Each experiment was performed in triplicate. Data are presented as the mean ± SD and analyzed by student's t-test (*p<0.05, **p<0.01, ***p<0.001)

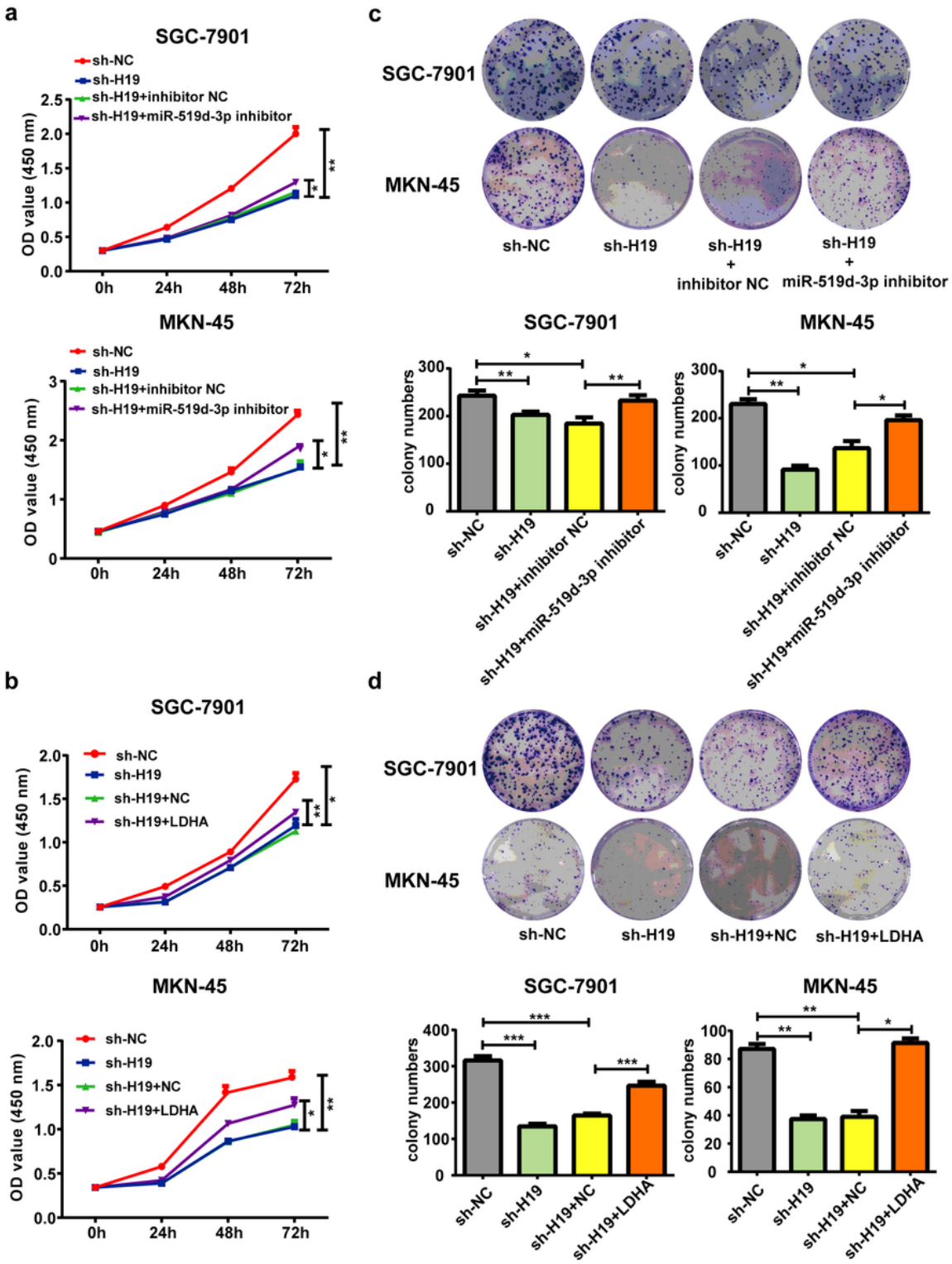

Figure 6

H19 knockdown suppressed GC cell proliferation via the miR-519d-3p/LDHA axis. a-b Cell viability of sh-H19 SGC-7901 and MKN-45 cells was analyzed by CCK8 kit after transfection with miR-519d-3p inhibitor (a) or LDHA overexpression plasmid (b). c-d Colony formation assay of sh-H19 SGC-7901 and MKN-45 cells after transfection with miR-519d-3p inhibitor (c) or LDHA overexpression plasmid (d). Each experiment was performed in triplicate. Data are presented as the mean ± SD and analyzed by student's t-test (*p<0.05, **p<0.01, ***p<0.001)

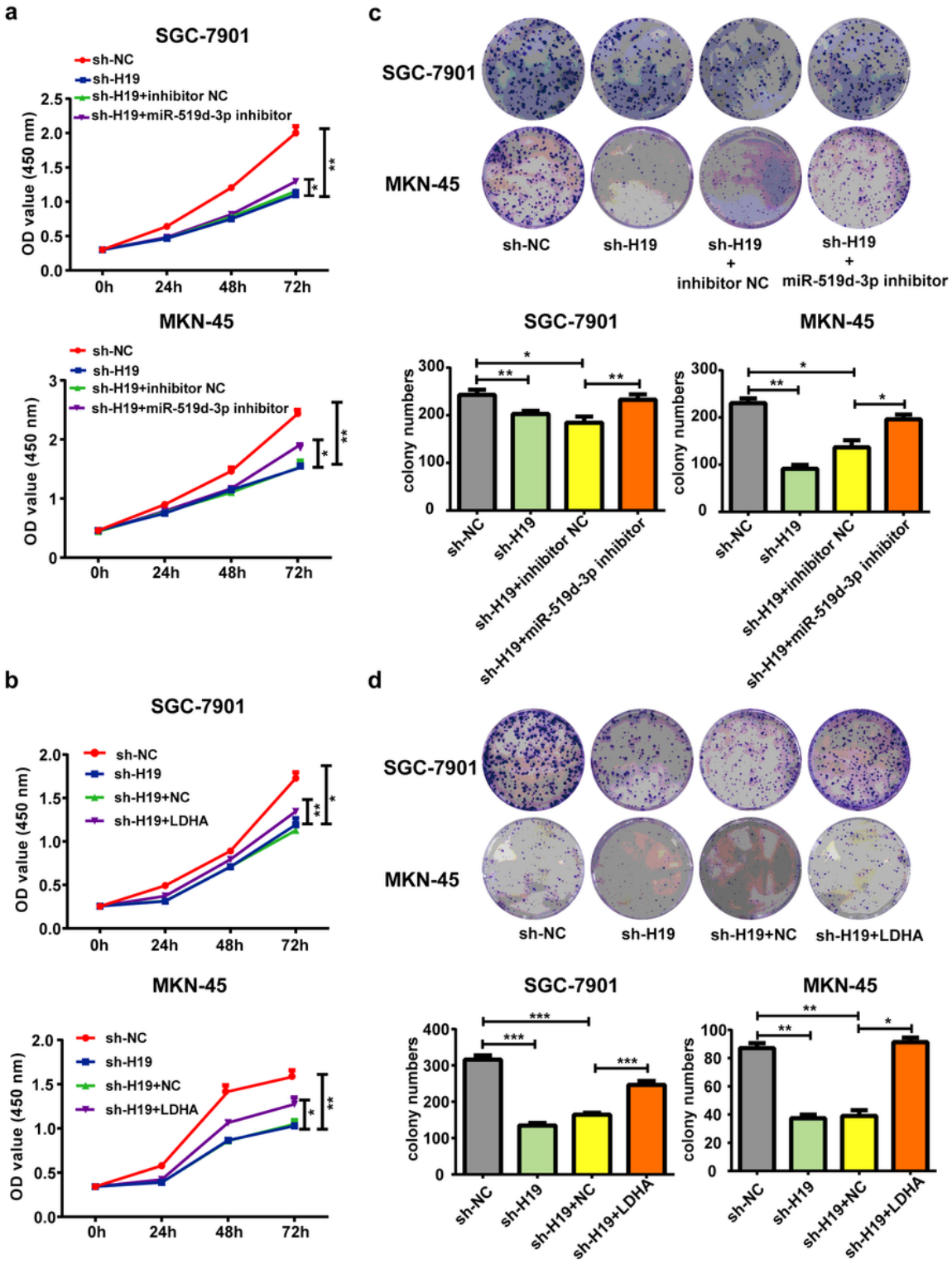

Figure 6

H19 knockdown suppressed GC cell proliferation via the miR-519d-3p/LDHA axis. a-b Cell viability of sh-H19 SGC-7901 and MKN-45 cells was analyzed by CCK8 kit after transfection with miR-519d-3p inhibitor (a) or LDHA overexpression plasmid (b). c-d Colony formation assay of sh-H19 SGC-7901 and MKN-45 cells after transfection with miR-519d-3p inhibitor (c) or LDHA overexpression plasmid (d). Each experiment was performed in triplicate. Data are presented as the mean ± SD and analyzed by student's t-test (*p<0.05, **p<0.01, ***p<0.001)

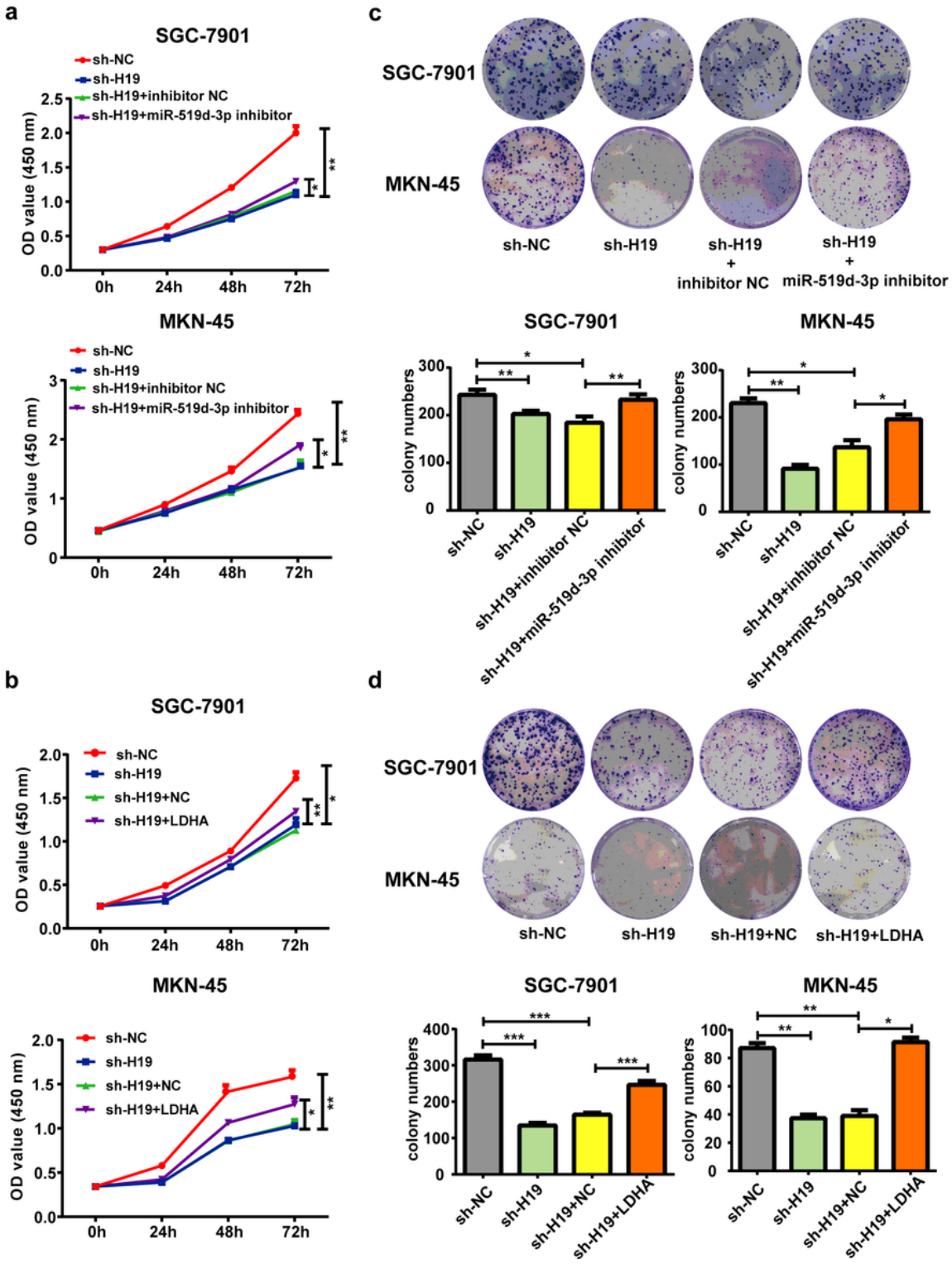

Figure 6

H19 knockdown suppressed GC cell proliferation via the miR-519d-3p/LDHA axis. a-b Cell viability of sh-H19 SGC-7901 and MKN-45 cells was analyzed by CCK8 kit after transfection with miR-519d-3p inhibitor (a) or LDHA overexpression plasmid (b). c-d Colony formation assay of sh-H19 SGC-7901 and MKN-45 cells after transfection with miR-519d-3p inhibitor (c) or LDHA overexpression plasmid (d). Each experiment was performed in triplicate. Data are presented as the mean ± SD and analyzed by student's t-test (*p<0.05, **p<0.01, ***p<0.001)

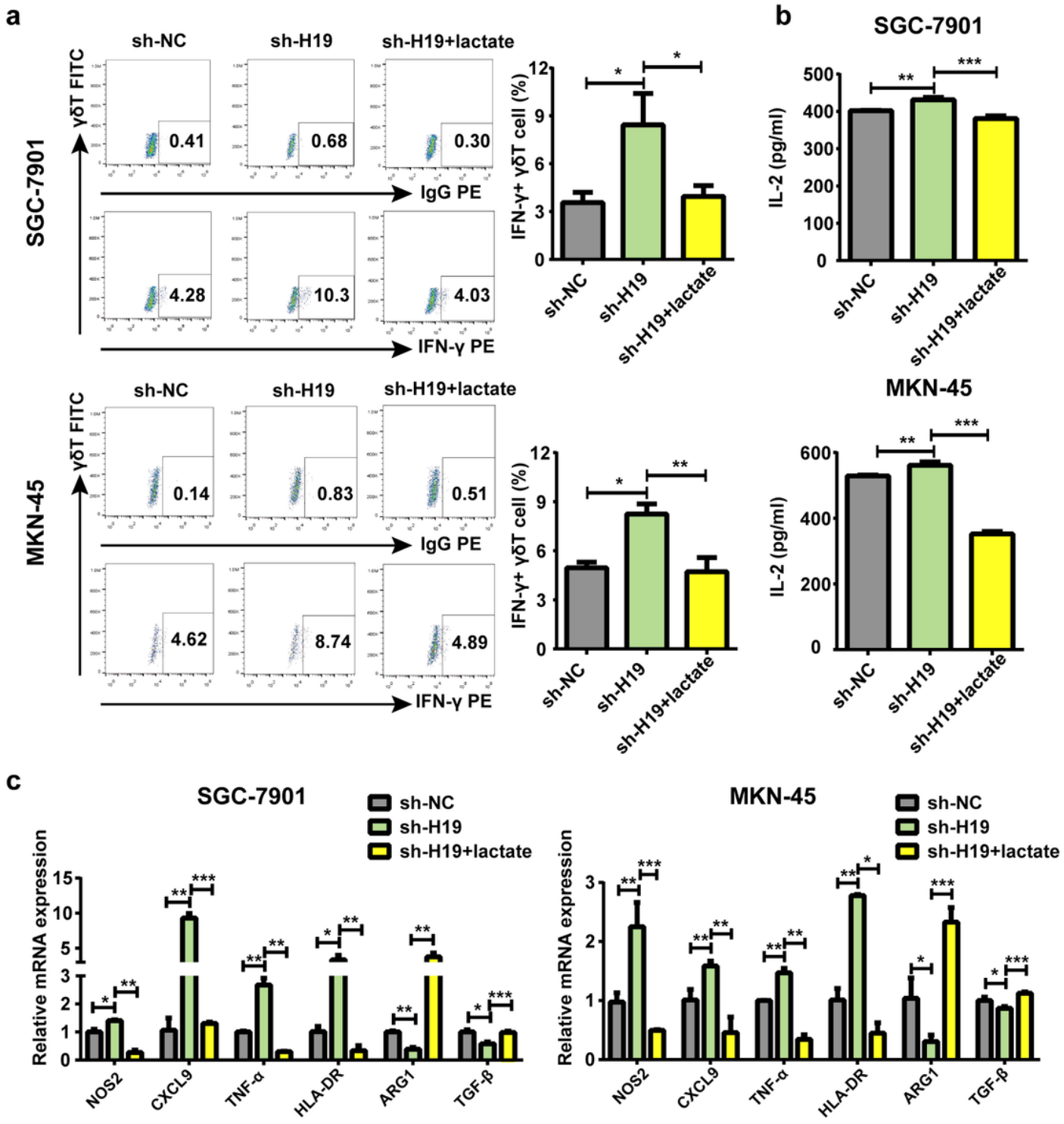

Figure 7

H19 knockdown affected tumor immune response via lactate. a The population of IFN-γ+ γδT cells among γδT cells co-treated with CM from sh-H19 SGC-7901 and MKN-45 cells and lactate was measured by flow cytometry. b The concentrations of IL-2 in the supernatants of PMA and Ionimycin-activated Jurkat cells co-treated with CM from sh-H19 SGC-7901 and MKN-45 cells and lactate. c The expression of the markers of M1 and M2 macrophages in PMA-treated THP-1 macrophages co-treated with CM from sh-H19 SGC-7901 and MKN-45 cells and lactate. Each experiment was performed in triplicate. Data are presented as the mean ± SD and analyzed by student's t-test (*p<0.05, **p<0.01, ***p<0.001)

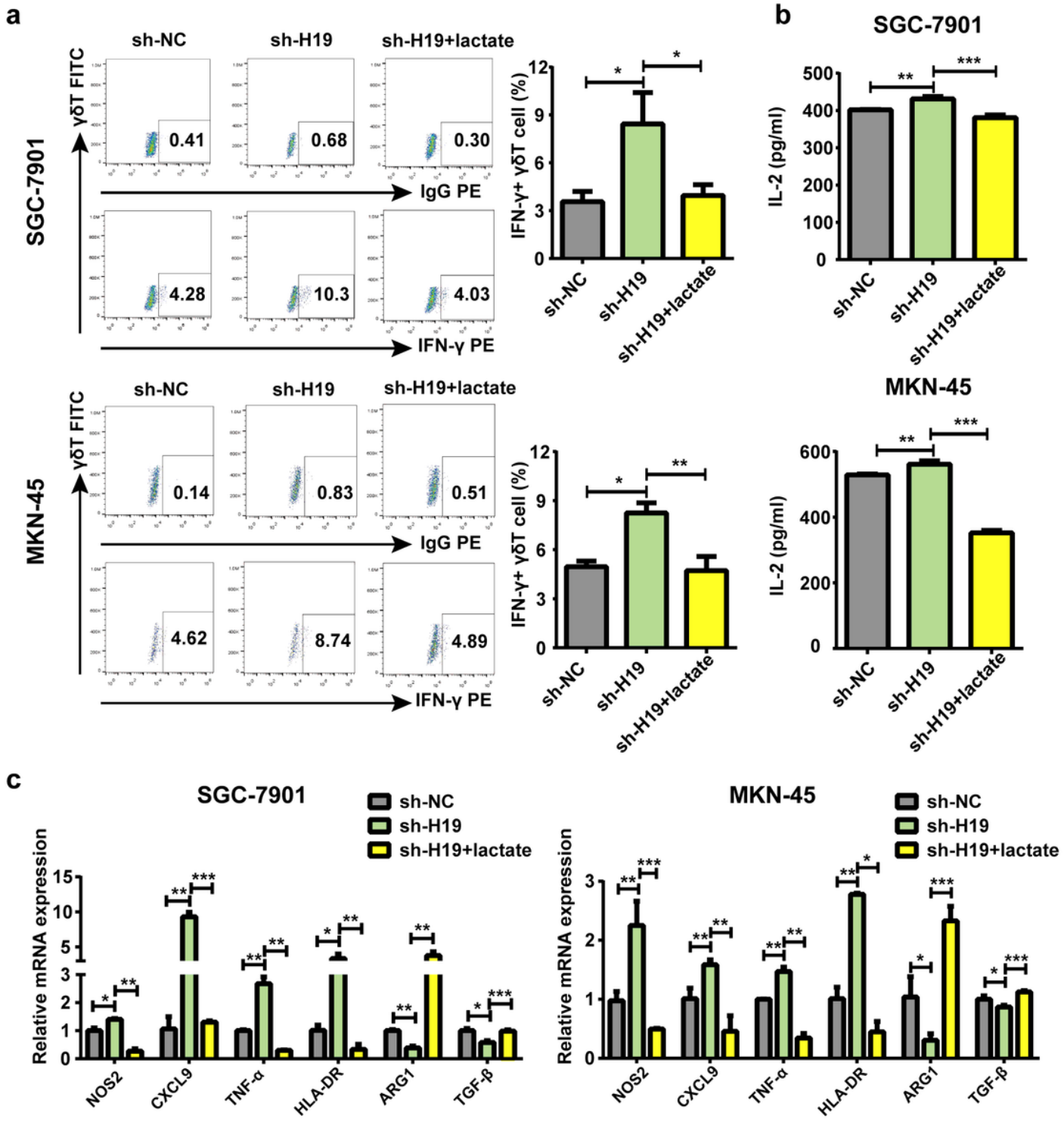

Figure 7

H19 knockdown affected tumor immune response via lactate. a The population of IFN-γ+ γδT cells among γδT cells co-treated with CM from sh-H19 SGC-7901 and MKN-45 cells and lactate was measured by flow cytometry. b The concentrations of IL-2 in the supernatants of PMA and Ionimycin-activated Jurkat cells co-treated with CM from sh-H19 SGC-7901 and MKN-45 cells and lactate. c The expression of the markers of M1 and M2 macrophages in PMA-treated THP-1 macrophages co-treated with CM from sh-H19 SGC-7901 and MKN-45 cells and lactate. Each experiment was performed in triplicate. Data are presented as the mean ± SD and analyzed by student's t-test (*p<0.05, **p<0.01, ***p<0.001)

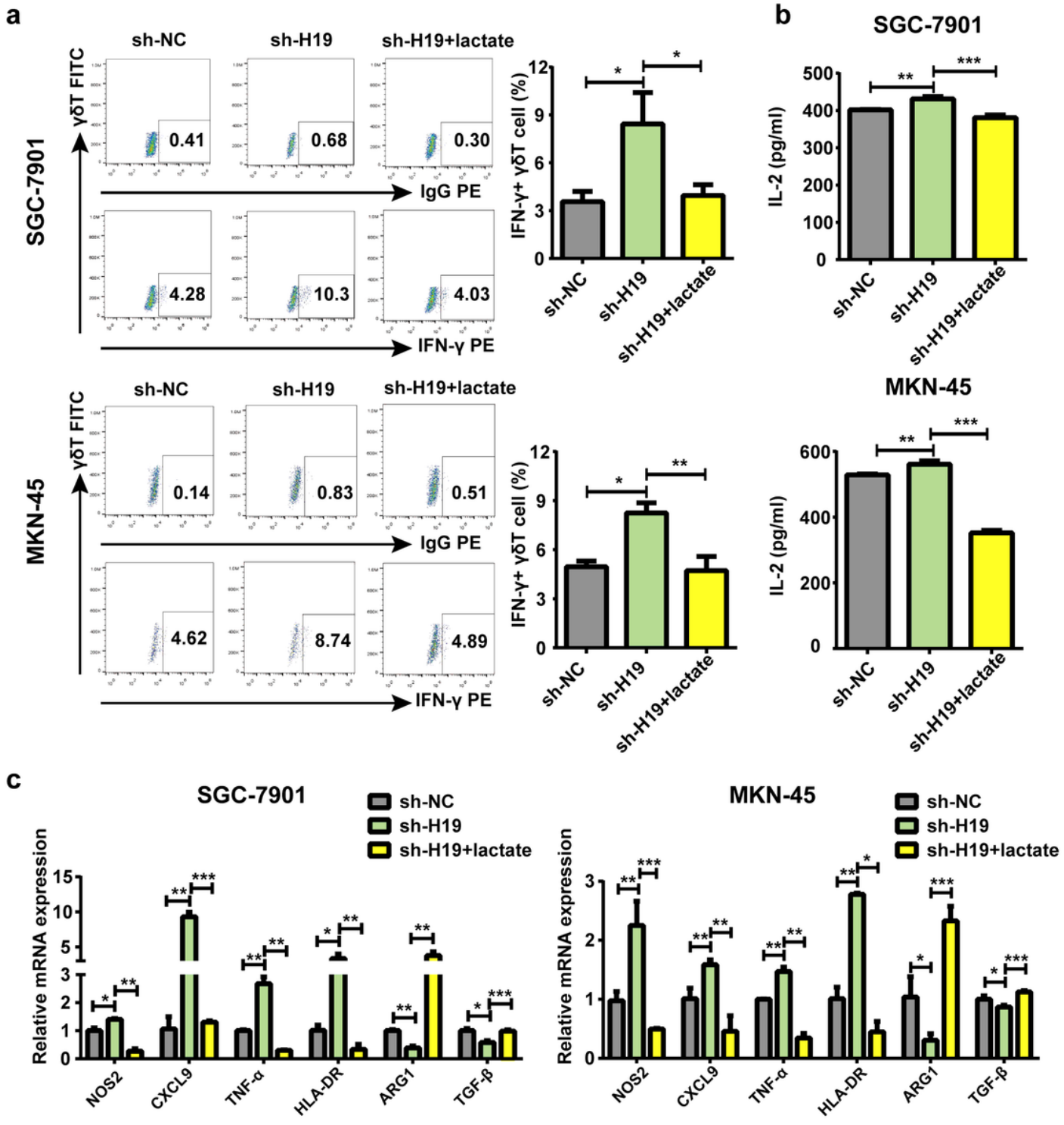

Figure 7

H19 knockdown affected tumor immune response via lactate. a The population of IFN-γ+ γδT cells among γδT cells co-treated with CM from sh-H19 SGC-7901 and MKN-45 cells and lactate was measured by flow cytometry. b The concentrations of IL-2 in the supernatants of PMA and Ionimycin-activated Jurkat cells co-treated with CM from sh-H19 SGC-7901 and MKN-45 cells and lactate. c The expression of the markers of M1 and M2 macrophages in PMA-treated THP-1 macrophages co-treated with CM from sh-H19 SGC-7901 and MKN-45 cells and lactate. Each experiment was performed in triplicate. Data are presented as the mean ± SD and analyzed by student's t-test (*p<0.05, **p<0.01, ***p<0.001)

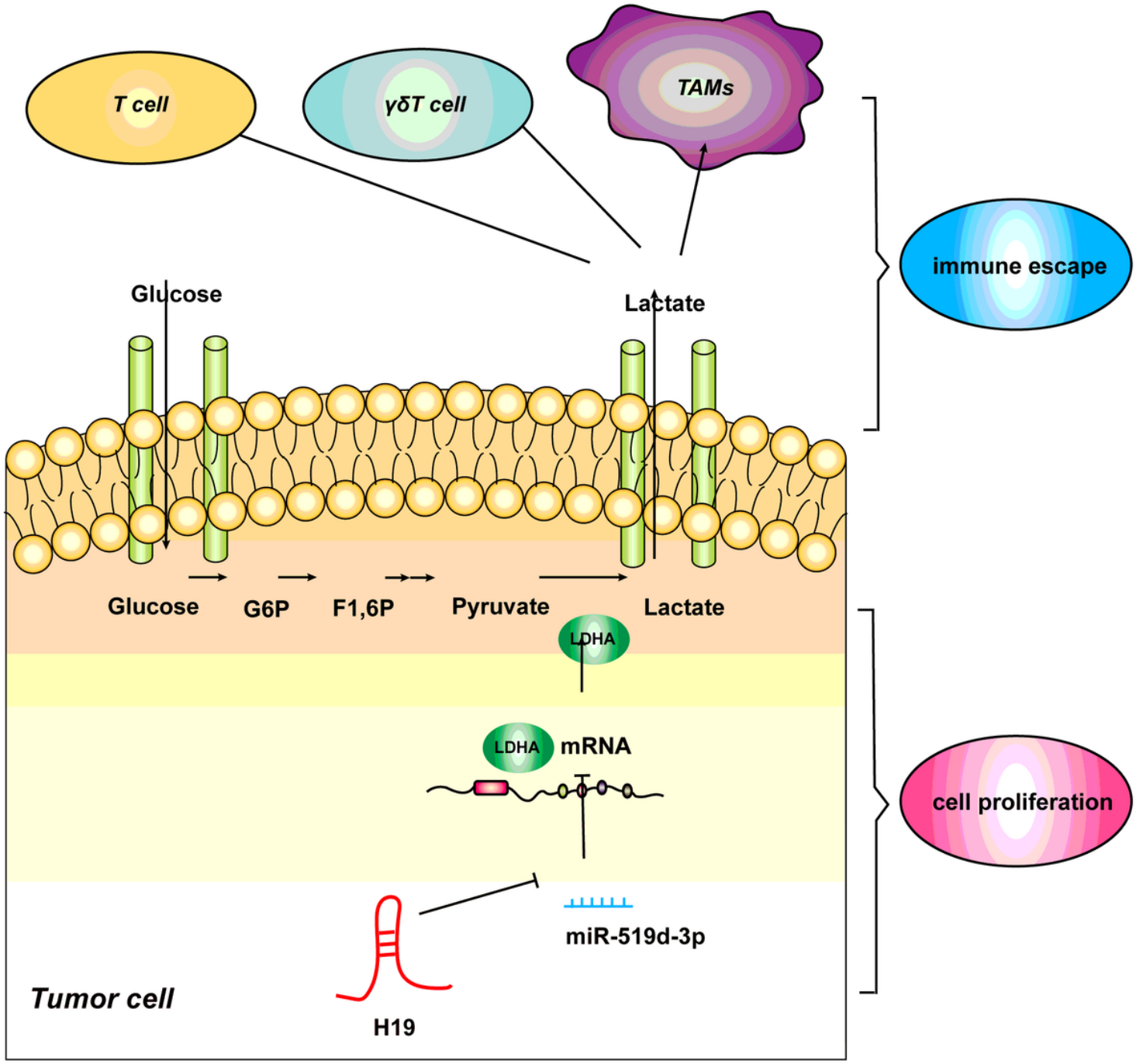

Figure 8

H19 modulated the aerobic glycolysis, proliferation, and immune escape of GC cells by sponging miR-519d-3p to induce the expression of LDHA.

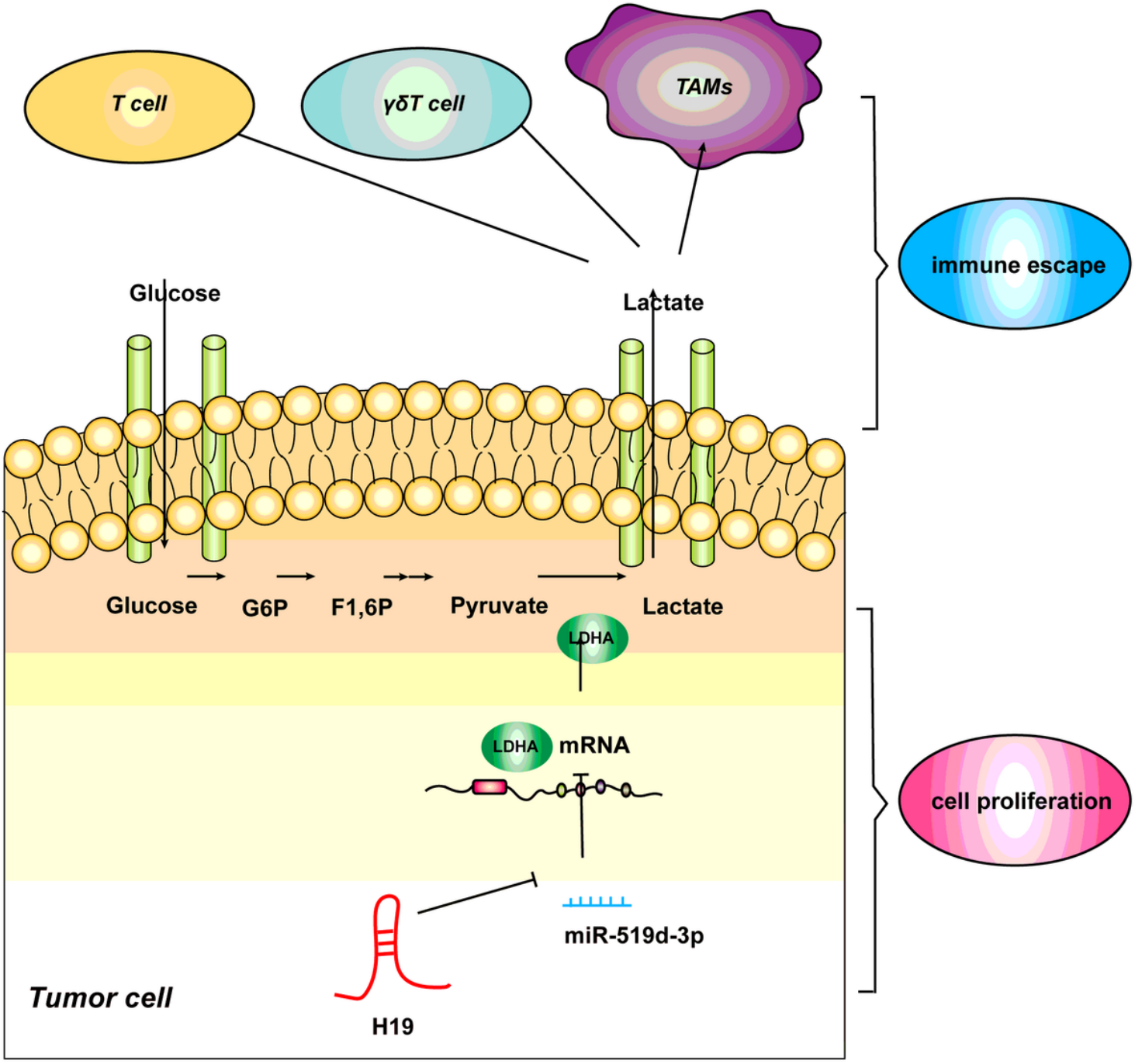

Figure 8

H19 modulated the aerobic glycolysis, proliferation, and immune escape of GC cells by sponging miR-519d-3p to induce the expression of LDHA.

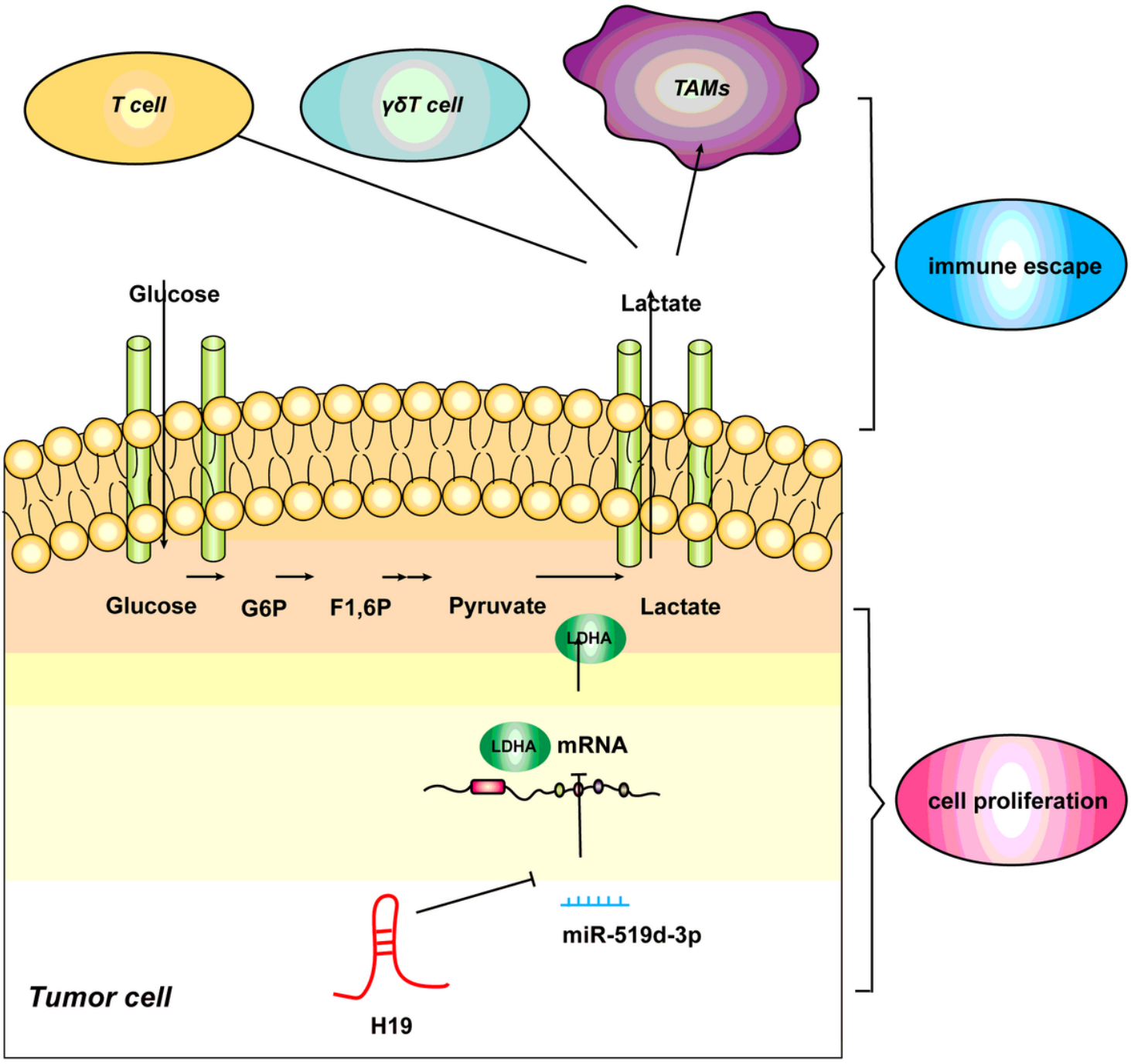

Figure 8

H19 modulated the aerobic glycolysis, proliferation, and immune escape of GC cells by sponging miR-519d-3p to induce the expression of LDHA.

Supplementary Files

This is a list of supplementary files associated with this preprint. Click to download.

- Additionalfile3.docx

- Additionalfile3.docx
- Additionalfile3.docx
- Additionalfile2.docx
- Additionalfile2.docx
- Additionalfile2.docx
- Additionalfile1.docx
- Additionalfile1.docx
- Additionalfile1.docx
- Fig.S4.tif
- Fig.S4.tif
- Fig.S4.tif
- Fig.S3.tif
- Fig.S3.tif
- Fig.S3.tif
- Fig.S2.tif
- Fig.S2.tif
- Fig.S2.tif
- Fig.S1.tif
- Fig.S1.tif
- Fig.S1.tif